Lab Invest 103 (2023) 100038

LABORATORY INVESTIGATION

journal homepage: https://laboratoryinvestigation.org/

Research Article

Role of Adrenomedullin 2/Intermedin in the Pathogenesis of Neovascular Age-Related Macular Degeneration

Shinji Kakihara[a,b], Yorishige Matsuda[a,b], Kazutaka Hirabayashi[a,b], Akira Imai[a,b], Yasuhiro Iesato[a,b], Takayuki Sakurai[a,c], Akiko Kamiyoshi[a,c], Megumu Tanaka[a], Yuka Ichikawa Shindo[a], Hisaka Kawate[a], Yunlu Zhao[a], Yan Zhang[a], QianQian Guo[a], Peixuan Li[a], Naho Onishi[a], Toshinori Murata[b], Takayuki Shindo[a,c,*]

[a] *Department of Cardiovascular Research, Shinshu University School of Medicine, Nagano, Japan;* [b] *Department of Ophthalmology, Shinshu University School of Medicine, Nagano, Japan;* [c] *Department of Life Innovation, Institute for Biomedical Sciences, Interdisciplinary Cluster for Cutting Edge Research, Shinshu University, Nagano, Japan*

ARTICLE INFO

Article history:
Received 14 October 2022
Revised 11 November 2022
Accepted 22 November 2022

Keywords:
adrenomedullin 2
laser induced choroidal neovascularization
mesenchyme homeobox 2
neovascular age related macular degeneration

ABSTRACT

Adrenomedullin 2 (AM2; also known as intermedin) is a member of the adrenomedullin (AM) peptide family. Similarly to AM, AM2 partakes in a variety of physiological activities. AM2 has been reported to exert protective effects on various organ disorders; however, its significance in the eye is unknown. We investigated the role of AM2 in ocular diseases. The receptor system of AM2 was expressed more abundantly in the choroid than in the retina. In an oxygen induced retinopathy model, physiological and pathologic retinal angiogenesis did not differ between AM2 knockout (AM2 /) and wild type mice. In contrast, in laser induced choroidal neovascularization, a model of neovascular age related macular degeneration, AM2 / mice had enlarged and leakier choroidal neovascularization lesions, with exacerbated subretinal fibrosis and macrophage infiltration. Contrary to this, exogenous admin istration of AM2 ameliorated the laser induced choroidal neovascularization associated pathology and suppressed gene expression associated with inflammation, fibrosis, and oxidative stress, including that of VEGF A, VEGFR 2, CD68, CTGF, and p22 phox. The stimulation of human adult retinal pigment epithelial (ARPE) cell line 19 cells with TGF β2 and TNF α induced epithelial to mesenchymal transi tion (EMT), whereas AM2 expression was also elevated. The induction of EMT was suppressed when the ARPE 19 cells were pretreated with AM2. A transcriptome analysis identified 15 genes, including mesenchyme homeobox 2 (Meox2), whose expression was significantly altered in the AM2 treated group compared with that in the control group. The expression of Meox2, a transcription factor that inhibits inflammation and fibrosis, was enhanced by AM2 treatment and attenuated by endogenous AM2 knockout in the early phase after laser irradiation. The AM2 treatment of endothelial cells inhibited endothelial to mesenchymal transition and NF κB activation; however, this effect tended to be canceled following Meox2 gene knockdown. These results indicate that AM2 suppresses the neo vascular age related macular degeneration related pathologies partially via the upregulation of Meox2. Thus, AM2 may be a promising therapeutic target for ocular vascular diseases.

Introduction

Angiogenesis, which is the formation of new blood vessels from preexisting vessels, plays a key role in various pathologic

* Corresponding author.
E-mail address: tshindo@shinshu-u.ac.jp (T. Shindo).

0023-6837/$ - see front matter © 2022 United States & Canadian Academy of Pathology. Published by Elsevier Inc. All rights reserved.
https://doi.org/10.1016/j.labinv.2022.100038

conditions, including ocular neovascular diseases and tumor formation.[1] An imbalance in the functions of various growth factors and cytokines in the eye compromises vascular ho meostasis. This leads to fragile pathologic neovascularization, such as retinal neovascularization (RNV) in proliferative diabetic retinopathy and choroidal neovascularization (CNV) in neo vascular age related macular degeneration (nAMD).[2-5] Both types of pathologic angiogenesis of the eye cause edema, bleeding, inflammation, and fibrosis in the fundus, leading to severe vision loss.[6,7] Currently, vascular endothelial growth factor (VEGF) is thought to be a major cause of pathologic ocular angiogenesis.[4] The prognosis of these diseases has been improved by employing photodynamic therapy with verteporfin and anti VEGF therapy. However, the effects of these treatments are transient and often result in recurrence and vision deteri oration; therefore, therapies that target molecules other than VEGF are under investigation.[8-10]

Adrenomedullin 2 (AM2), also known as intermedin, is a member of the calcitonin superfamily.[11] AM2 is widely expressed throughout the body and in the circulatory, repro ductive, and digestive systems, adipose tissue, and kidneys. AM2 exhibits various functions, including vasodilation and positive inotropic, natriuretic, and angiogenic effects. Further more, AM2 alleviates endoplasmic reticulum and oxidative stress in phosphatidylinositol 3 kinase/Akt and extracellular signal regulated kinase−dependent pathways. As a result, it plays a protective role against various organ disorders.[11,12] AM2 has also been reported to suppress excessive vessel sprouting by both restraining the endothelial cell response to VEGF and inducing endothelial cell proliferation and vascular lumen enlargement. These actions lead to vascular remodeling, resulting in a hierarchical vasculature, and vascular normaliza tion in tumor angiogenesis models[13-15]; however, the effects of AM2 on ocular pathologic angiogenesis have not been eluci dated yet.

Two models are frequently used to investigate the mecha nisms underlying the development of pathologic angiogenesis in the eye. One model is oxygen induced retinopathy (OIR),[16] designed to investigate RNV under hypoxia, and the other is laser induced CNV (LI CNV),[17] which is a model of nAMD. The mechanisms underlying RNV and CNV have common aspects, such as the effectiveness of anti VEGF therapy, whereas other aspects differ.[18] In OIR, the transition from hyperoxia to nor moxia causes ischemia in the retina, which may cause patho logic RNV.[19] In contrast, various factors, including genetic background, inflammation, integrity of the extracellular matrix, lipids, and dietary antioxidants, can play important roles in the pathophysiology of CNV.[20,21]

This study aimed to investigate the role of AM2 in ocular pathologic angiogenesis and its underlying mechanisms using exogenous administration and endogenous knockout of AM2 in mouse OIR and LI CNV models. We found that AM2, unlike its peptide family member AM,[22] had no apparent effect on pathologic RNV in the OIR model; however, it alleviated nAMD related pathogeneses, including the disruption of the blood retina barrier, CNV formation, inflammation, and fibrosis. AM2 inhibited epithelial to mesenchymal transition (EMT) and endothelial to mesenchymal transition (EndMT), which are the major causes of subretinal fibrosis. Furthermore, we found that the mesenchyme homeobox 2 (Meox2) tran scription factor, which suppresses fibrosis and inflammation, may be a candidate target factor for the beneficial effects of AM2 on LI CNV.[23-26]

Materials and Methods

Experimental Animals

AM2 knockout (AM2 /) mice were generated in our labora tory using the clustered regularly interspaced short palindromic repeats (CRISPR)/CRISPR associated protein 9 system. The AM2 / strain was established in C57BL/6J mice and underwent backcross breeding. All mice were maintained according to a strict procedure under specific pathogen free conditions in an environmentally controlled (12 h light/dark cycle; room tem perature, 22 ± 2 °C) breeding room at the Division of Laboratory Animal Research, Department of Life Science, Research Center for Human and Environmental Sciences, Shinshu University. All experiments were performed in accordance with the Association for Research in Vision and Ophthalmology's Statement for the Use of Animals in Ophthalmic and Vision Research and approved by the Ethics Committee of Shinshu University School of Medi cine (approval numbers: 021038 1 and 021038 2). Prior to all invasive procedures, the mice were anesthetized through intra peritoneal injection of a combination anesthetics that included 0.3 mg/kg medetomidine (Nippon Zenyaku Kogyo), 4.0 mg/kg midazolam (Astellas Pharma), and 5.0 mg/kg butorphanol (Meiji Seika Pharma).

Physiological Angiogenesis in Neonates

On postnatal day 7 (P7), the mice were euthanized by cervical dislocation, their eyes were removed, and flat mounted retinal specimens were prepared. They were stained with isolectin B4 (isolectin GS IB4 from *Griffonia simplicifolia*, Alexa Fluor 488 or 594 conjugates; 1:200; Invitrogen) and examined as previously described.[27,28] In brief, the eyes were fixed in 4% para formaldehyde for 1 hour and washed with phosphate buffered saline (PBS). The retinas were then isolated and stained over night at 4 °C with isolectin B4 in PBS with 0.3% Triton X 100. After washing the specimens with PBS, approximately 4 radial cuts were made from the edges to the equators. The specimens were mounted onto microscope slides embedded in a fluorescent mounting medium (Agilent Technologies).

Images of the retinas were acquired using a fluorescence mi croscope (BZ X710; Keyence), and the superficial vascular devel opment in the retina was quantified. Vascular progression was measured by defining a straight line from the angiogenic front to the center of each retinal quadrant. The number of vessel branch points and the vascular density of the area near the developing vascular front on P7 were quantified using the AngioTool image analysis software version 0.6a (National Cancer Institute).[29]

Oxygen Induced Retinopathy Model

Ischemic retinopathy and pathologic RNV were induced in mice to establish the OIR model as previously described by Smith et al.[16] In brief, mice from P7 were exposed to 75% oxygen for 5 days using a chamber with a ProOx110 oxygen control device (BioSpherix) and placed in atmospheric air to induce RNV. Retinal flat mounts were prepared in a manner similar to that in the physiological angiogenesis model in neonatal mice, and retinal angiogenesis was quantified as described previously.[19] The avas cular area and neovascular tuft formation (regarded as pathologic

Table 1
Primers used for real-time quantitative PCR

Primer	Sequence
m *Adm* (AM) Forward	5′-GGACACTGCAGGGCCAGAT-3′
m *Adm* (AM) Reverse	5′-GTAGTTCCCTCTTCCCACGACTTA-3′
m *Adm2* (AM2) Forward	5′-AGGCACTCCAGACCCAGAGA-3′
m *Adm2* (AM2) Reverse	5′-AGGGAAGGGTGTCCAGGCT-3′
m *Calca* (CGRP) Forward	5′-TCCTGCAACACTGCCACCT-3′
m *Calca* (CGRP) Reverse	5′-ACACCTCCTGATCTGCTCAGC-3′
m *Calcrl* (CLR) Forward	5′-AGGCGTTTACCTGCACACACT-3′
m *Calcrl* (CLR) Reverse	5′-CAGGAAGCAGAGGAAACCCC-3′
m *Ramp1* Forward	5′-GCACTGGTGGTCTGGAGGA-3′
m *Ramp1* Reverse	5′-CCCTCATCACCTGGGATACCT-3′
m *Ramp2* Forward	5′-ACTGAGGACAGCCTTGTGTCAAA-3′
m *Ramp2* Reverse	5′-CCTTGACAGAGTCCATGCAACTC-3′
m *Ramp3* Forward	5′-AAAGCCTTCGCTGACATGATG-3′
m *Ramp3* Reverse	5′-ATCTCGGTGCAGTTAGTGAAGCT-3′
m *Vegfa* Forward	5′-GCAGGCTGCTGTAACGATGA-3′
m *Vegfa* Reverse	5′-CGCATGATCTGCATGGTGAT-3′
m *Cd68* Forward	5′-TGGCGGTGGAATACAATGTG-3′
m *Cd68* Reverse	5′-GAGATGAATTCTGCGCCATGA-3′
m *Il6* Forward	5′-CCCAATTTCCAATGCTCTCC-3′
m *Il6* Reverse	5′-TGAATTGGATGGTCTTGGTCC-3′
m *Tnf* (TNF-α) Forward	5′-ACGGCATGGATCTCAAAGAC-3′
m *Tnf* (TNF-α) Reverse	5′-AGATAGCAAATCGGCTGACG-3′
m *Cyba* (p22-phox) Forward	5′-GGCCATTGCCAGTGTGATCT-3′
m *Cyba* (p22-phox) Reverse	5′-GCTCAATGGGAGTCCACTGC-3′
m *Ncf1* (p47-phox) Forward	5′-ATCCTATCTGGAGCCCCTTGA-3′
m *Ncf1* (p47-phox) Reverse	5′-CACCTGCGTAGTTGGGATCC-3′
m *Ncf2* (p67-phox) Forward	5′-CAGACCCAAAACCCCAGAAA-3′
m *Ncf2* (p67-phox) Reverse	5′-AAAGCCAAACAATACGCGGT-3′
m *Tgfb1* Forward	5′-CCCGAAGCGGACTACTATGC-3′
m *Tgfb1* Reverse	5′-TAGATGGCGTTGTTGCGGT-3′
m *Ccn2* (CTGF) Forward	5′-CAGAGGTGGTGGGGTAGAGA-3′
m *Ccn2* (CTGF) Reverse	5′-CATTGCCACTCACAATGTCC-3′
m *Kdr* (VEGFR-2) Forward	5′-ACTGCAGTGATTGCCATGTTCT-3′
m *Kdr* (VEGFR-2) Reverse	5′-TCATTGGCCCGCTTAAGG-3′
m *Il1b* Forward	5′-CTACAGGCTCCGAGATGAACAAC-3′
m *Il1b* Reverse	5′-TCCATTGAGGTGGAGAGCTTTC-3′
m *Meox2* Forward	5′-GAGGACAGCCGCGATAGTG-3′
m *Meox2* Reverse	5′-AGAATGGAGCTGGTCTTTGTAGGT-3′
m *Vcam1* Forward	5′-CCCTGAATACAAAACGATCGC-3′
m *Vcma1* Reverse	5′-CAGCCCGTAGTGCTGCAAG-3′
m *Serpine1* (PAI-1) Forward	5′-ACCAAGAGCAGCTCTCTGTAGCA-3′
m *Serpine1* (PAI-1) Reverse	5′-CTTGGCCCATGAAGAGGATTGTCT-3′
m *Fn1* (Fibronectin 1) Forward	5′-GGCTACATCATCCGCCATCA-3′
m *Fn1* (Fibronectin 1) Reverse	5′-GCCCGGATTAAGGTTGGTGA-3′
m *Angpt1* Forward	5′-CATGGGCAATGTGCCTACAC-3′
m *Angpt1* Reverse	5′-TCGCACTCTCACGGCAGTT-3′
m *Angptl1* Forward	5′-ACCACCTGATCTGCCAACAGCT-3′
m *Angptl1* Reverse	5′-CTGAGTGTCCAGCTTCCTTTGC-3′
h *Adm2* (AM2) Forward	5′-TCCTGCAGCAACAATACCTGC-3′
h *Adm2* (AM2) Reverse	5′-GGGTGTTTAGGCTCCTTGACG-3′
h *Adm* (AM) Forward	5′-AGACAGCAGTCCGGATGCC-3′
h *Adm* (AM) Reverse	5′-AGTTGTTCATGCTCTGGCGG-3′
h *Tagln* (SM22α) Forward	5′-GATTTTGGACTGCACTTCGC-3′
h *Tagln* (SM22α) Reverse	5′-GTCCGAACCCAGACACAAGT-3′
h *Meox2* Forward	5′-GTCAGAAGTCAACAGCAAACCCAG-3′
h *Meox2* Reverse	5′-CACATTCACCAGTTCCTTTTCCCGAGCC-3′

RNV) were quantified using Adobe Photoshop CS5 (Adobe Systems).

For the exogenous administration experiments, P12 wild type (WT) mice were anesthetized by intraperitoneal injection of a mixture of medetomidine, midazolam, and butorphanol. The mice were then treated with intravitreal injection of 1.5 μL of PBS, AM (10^{-7} mol/L, human AM; Peptide Institute) dissolved in PBS, or AM2 (10^{-7} mol/L, human AM2; Peptide Institute) dissolved in PBS, using a Hamilton syringe equipped with a 33 gauge needle. After the treatment, 3.0 mg/kg atipamezole (ZEOAQ) was intraperitoneally injected to reverse the anesthesia.

Laser Induced Choroidal Neovascularization Model

Male mice aged between 9 and 12 weeks were used in this experiment. The pupils of the right eye were dilated with one drop of 0.5% tropicamide and 0.5% phenylephrine (Mydrine P; Santen). The mice were anesthetized in a manner similar to that in the OIR model. CNV was then induced in the right eye as previously described.[30] The Bruch membrane was ruptured using laser photocoagulation to induce CNV using a laser slit lamp (GYC 1000; NIDEK) and a cover glass with a viscoelastic substance as the contact lens. A laser was used with the following parameters: wavelength, 532 μm; power output, 200 mW; spot size, 50 μm, and laser exposure duration, 50 ms. Laser injuries were generated in an area without obvious retinal vessels around the optic disc. The rupture of the Bruch membrane was confirmed by the appearance of air bubbles. Three or 4 shots per eye was used to evaluate CNV, and 5 shots per eye was used to extract the total RNA. After the treatment, 3.0 mg/kg atipamezole was intraperitoneally injected to reverse the anesthesia.

The AM and AM2 administration experiments were performed by either systemic or local administration. For systemic administration, AM and AM2 were infused subcutaneously using an osmotic pump (Alzet; DURECT) immediately after laser irradiation. The infusion condition was 1.2 μg/kg/h for 7 days, and the dosage was selected based on previously reported studies.[31,32] For local administration, AM and AM2 (10^{-7} mol/L; 1.0 μL) were injected intravitreally immediately after laser irradiation using a Hamilton syringe equipped with a 30 gauge needle under a surgical microscope at the corneal scleral junction.

Fluorescein Isothiocyanate Dextran Perfusion and Immunostaining of Choroidal Flat Mounts

The CNV lesions were measured in choroidal flat mounts as previously described.[33] On day 7 or 14 after laser irradiation, the mice were anesthetized and perfused with 1 mL of PBS containing 50 mg/mL fluorescein isothiocyanate (FITC) labeled dextran (FITC dextran; molecular weight, 2×10^6; Sigma Aldrich) from the left ventricle. The eyes were enucleated and fixed for 1 hour in 4% paraformaldehyde, the cornea and lens were removed, and the entire retina was dissected from the eyecup. Approximately 8 radial cuts were made from the edges to the equators of the specimens and mounted onto a slide glass. FITC positive areas represented the CNV areas.

For immunostaining, after blocking with 1% bovine serum albumin, the specimens were incubated with rabbit anti mouse α smooth muscle actin (α SMA; Abcam) and rat anti mouse F4/80 (Bio Rad) primary antibodies, followed by the appropriate secondary antibodies. Flat mounts were examined using a fluorescence microscope (BZ X710; Keyence). The sizes of the CNV lesions and α SMA positive areas were quantified using the analytic application BZ X analyzer (Keyence). The number of F4/80 positive cells in each CNV lesion was counted using a double blinded method for quantification. In the choroidal flat mount analysis, n represented the number of CNV lesions.

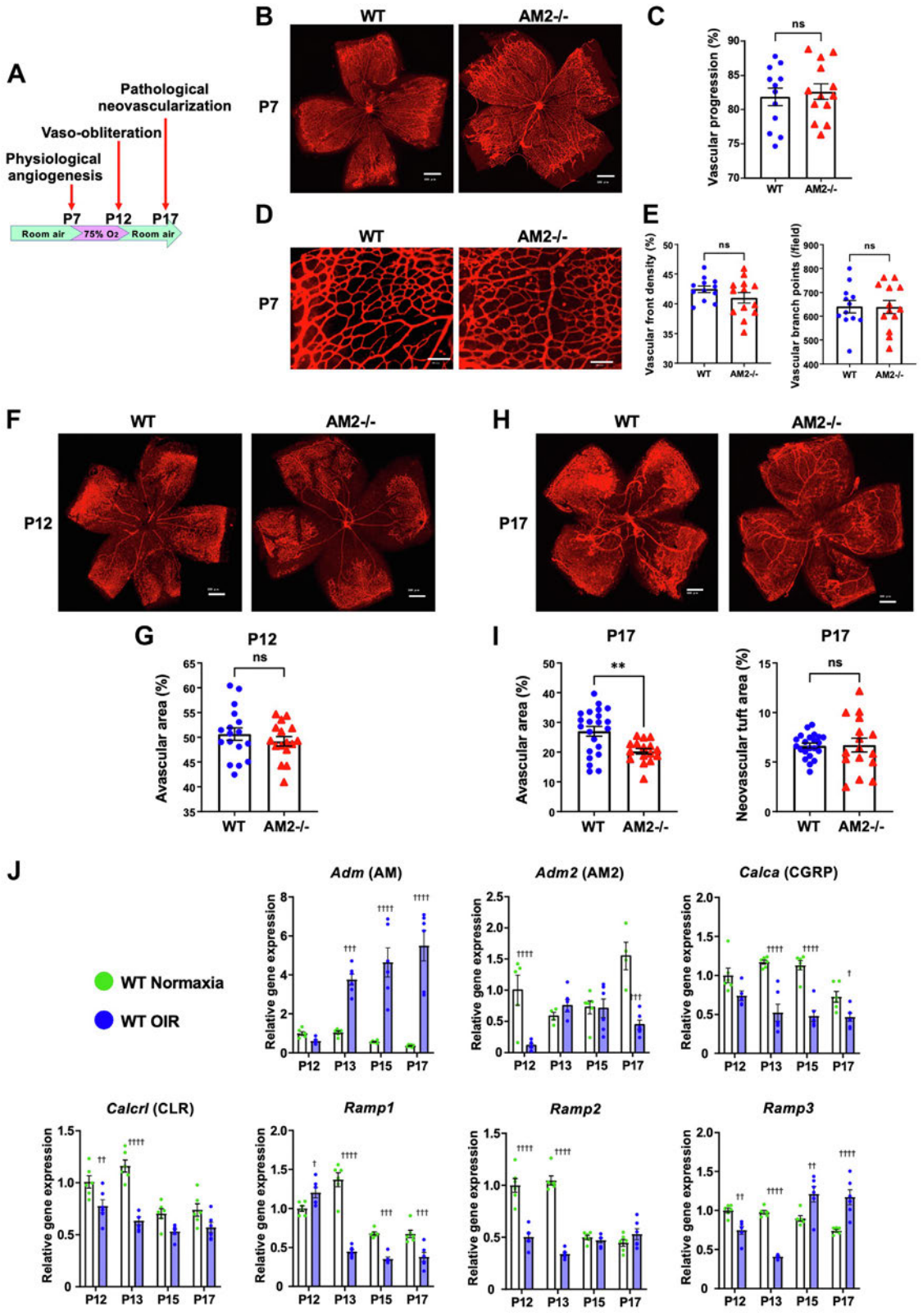

Figure 1.

Evaluation of retinal physiological angiogenesis and oxygen-induced retinopathy (OIR) in adrenomedullin 2-knockout (AM2-/-) and wild-type (WT) neonates. (A) Time course schematic of the mouse OIR model. We evaluated physiological angiogenesis on postnatal day 7 (P7), vaso-obliteration on P12, and pathologic neovascularization on P17. (B) Representative lectin-stained flat-mount retina on P7. Scale bar 500 μm. (C) Bar graph comparing the percentage of vascular progression in the superficial retinal layer. Vascular progression was defined by a straight line from the angiogenic front to the center of the retina. (D) Representative lectin-stained vessel images showing areas near the developing vascular front on P7. Scale bar 100 μm. (E) Bar graphs comparing the percentage of vascular front density and the number of vascular branch points per field (magnification: ×40) in the area near the developing vascular front. (F) Representative lectin-stained flat-mount retina on P12. Scale bar 500 μm. (G) Bar graph comparing the

Pathologic Sections

The eyes were enucleated, fixed in 4% paraformaldehyde overnight, and embedded in paraffin, after which 5 μm thick sections were prepared for histologic analyses. The sections were stained with hematoxylin eosin and immunostained with anti α SMA antibody (Agilent Technologies) and anti Meox2 antibody (Sigma Aldrich).

Fluorescein Angiography

Fluorescein angiography (FA) was performed in the LI CNV mouse model 7 days after laser irradiation. The AM2 administration experiment was performed using systemic administration. To evaluate vascular leakage, we photographed the fluorescence at early (2 3 minutes) and late (5 6 minutes) periods after intraperitoneal injection of 0.1 mL of 1% fluorescein sodium (Alcon) and compared the severity of the leakage between the time ranges. We graded the severity of the leakage using the following previously described scale[34]: grade 0 (no leakage), no leakage, faint, or mottled fluorescence without leakage; grade 1 (questionable leakage), a hyperfluorescent lesion with no progressive increase in size or intensity; grade 2 (leakage), increase in fluorescence intensity, but not size, with no definite leakage; and grade 3 (pathologically significant leakage), increase in both fluorescence area and intensity. In the FA analysis, n represented the number of laser applications to induce CNV.

Transendothelial Fluorescein Isothiocyanate Dextran Permeability and Transendothelial Electrical Resistance Analysis

TR iBRB cells (FACT) from a conditionally immortalized rat retinal capillary endothelial cell line generated from rats harboring temperature sensitive SV40 antigens were used for this experiment. TR iBRB cells were cultivated in Dulbecco modified Eagle medium supplemented with 10% fetal bovine serum and penicillin/streptomycin at 33 °C in an atmosphere of 5% CO_2.

To measure the monolayer transendothelial FITC permeability (TEFP) and transendothelial electrical resistance (TEER), TR iBRB cells were grown on CORNING BioCoat collagen I 24 well clear multiwell plates (CORNING) and Falcon cell culture inserts (pore size, 1.0 μm) (CORNING). The cells were plated at a density of 1.0×10^5 cells/well (upper compartment) and cultured for 3 days, at which point they formed a tight monolayer. Afterward, 0.2 mL and 1.2 mL of the medium were added to the upper and lower compartments (inside and outside the membrane inserts, respectively). Then, 10^{-8} to 10^{-6} mol/L of AM2 was added to the incubation medium (upper compartment), and after the pretreatment of AM2 for 24 hours, 20 ng/mL VEGF A (Sigma Aldrich) was added to the upper compartment.

For measuring the TEFP, the cells were incubated in the medium for 60 minutes, followed by the addition of FITC dextran (molecular weight, 4×10^3) (Sigma Aldrich) to the upper compartment for 180 minutes. Then, 50 μL of the medium was collected from the lower compartment. The fluorescence intensity of each sample was evaluated using a microplate fluorometer (Perkin Elmer multimode palate reader ARVO X4; Perkin Elmer) at excitation and emission wavelengths of 485 and 535 nm, respectively, and an integration time of 0.1 seconds.

The TEER was measured at 180 minutes using a Millicell ERS2 Epithelial Volt/Ohm Meter system (Merck Millipore). The measured TEER included the resistance of the interelectrode solution and blank membrane. Therefore, a culture well without cells was included as a blank.

These experiments were performed using an optimized and slightly modified version of previously published methods.[32,35] Every test was repeated at least 3 times.

Induction of Epithelial to Mesenchymal Transition in Retinal Pigment Epithelial Cells

Immortalized adult retinal pigment epithelial cell line 19 (ARPE 19) cells were purchased from American Type Culture Collection. The cells were cultured in Dulbecco modified Eagle medium/Ham nutrient mixture F 12 supplemented with 10% fetal bovine serum and penicillin/streptomycin at 37 °C in an atmosphere of 5% CO_2. To induce retinal pigment epithelial disruption or EMT, transforming growth factor (TGF) β2 (5 ng/mL) (Sigma Aldrich) and tumor necrosis factor (TNF) α (10 ng/mL) (Sigma Aldrich) were added before the cells reached confluence. AM2 (10^{-7} or 10^{-9} mol/L) was added 24 hours before the addition of TGF β2 and TNF α. The dose and treatment period were selected based on previous studies that used AM.[31,36,37] After 48 hours of induction of EMT, the cells were fixed in 4% paraformaldehyde for 10 minutes, blocked, and immunostained with anti zonula occludens protein 1 (ZO 1) (BD Biosciences), anti smooth muscle 22α (anti SM22α) (Abcam), and anti collagen α1 (Novus Biologicals) antibodies. The cells were also stained with phalloidin (Thermo Fisher Scientific) to visualize actin fibers and were then examined using a microscope (BZ X710). The ZO 1 stained images were subjected to haze reduction under the same conditions to identify the ZO 1 positive areas around the cell boundaries. Positive areas were determined using the Hybrid Cell Count software(Keyence) under the same conditions for each staining. Every test was repeated at least 3 times.

RNA Extraction and Real Time Quantitative Reverse Transcription PCR Analysis

The mice were euthanized, and their eyes were enucleated. The cornea, iris, lens, vitreous, and surrounding soft tissues were removed. The retina and the retinal pigment epithelium choroid sclera complex were separated, and specimens of each were collected. Total RNA was extracted from the retina, choroidal complexes, and cells using TRI reagent (MRC), and 1 μg of the extracted RNA was treated using RT^2 First Strand kit (Qiagen) to remove contaminating genomic DNA and synthesize complementary DNA. Real time quantitative reverse transcription PCR (qPCR) was performed using a StepOnePlus real time

percentage of avascular area in the whole retina on P12. (H) Representative lectin-stained flat-mount retina on P17. Scale bar 500 μm. (I) Bar graphs comparing the percentages of vascular and neovascular tuft areas within the whole retina on P17. Bars indicate the mean ± SEM. $^{**}P < .01$; *P* values were calculated using the Mann Whitney *U* test (C, E, G, and I). (J) Quantitative real-time PCR analysis of the time course of the gene expression of calcitonin super family peptides and their receptor components in the mouse OIR model. Means of the WT mice on P12 were assigned a value of 1. Bars indicate the mean ± SEM. $^{\dagger}P < .05$, $^{\dagger\dagger}P < .01$, $^{\dagger\dagger\dagger}P < .001$, and $^{\dagger\dagger\dagger\dagger}P < .0001$ (compared with WT); *P* values were calculated using the 2-way analysis of variance with the Kruskal Wallis test (J). AM, adrenomedullin; CGRP, calcitonin gene-related peptide; CLR, calcitonin receptor-like receptor; RAMP, receptor activity-modifying protein.

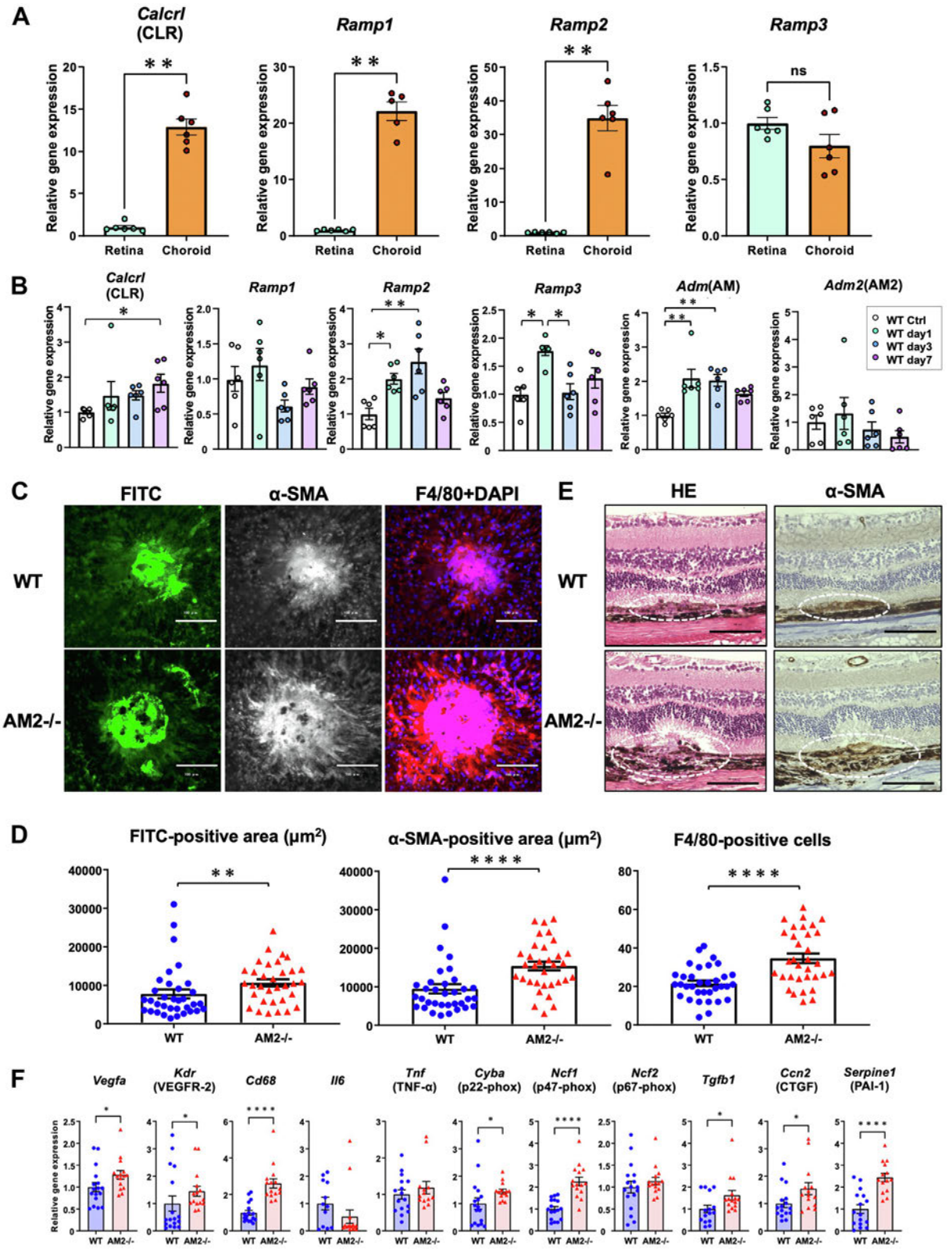

Figure 2.

Evaluation of laser-induced choroid neovascularization (LI-CNV) in adrenomedullin 2-knockout (AM2-/-) and wild-type (WT) mice. (A) Quantitative real-time PCR analysis comparing the gene expression of the receptor components of AM2 between the retina and the choroid. Means of retina were assigned a value of 1. CLR, receptor activity-modifying protein 1 (RAMP1), and RAMP2 were expressed more in the choroid than in the retina. (B) Quantitative real-time PCR analysis of the gene expression of AM, AM2, and their receptor components in the choroid of untreated control WT mice and WT mice on days 1, 3, and 7 after laser irradiation. Means of control mice were assigned a value of 1. (C) Comparison of LI-CNV between AM2-/- and WT mice. On day 7, after laser-induced injury to the Bruch membrane, choroidal flat mounts were prepared, the fluorescein isothiocyanate (FITC)-positive CNV and α-SMA-positive fibrotic areas were measured, and the number of F4/80-positive macrophages were

PCR system (Thermo Fisher Scientific), SYBR Green (Toyobo), and real time PCR master mix (Toyobo). Glyceraldehyde 3 phosphate dehydrogenase (Thermo Fisher Scientific) expression was used as the endogenous control. Table 1 shows the primers used, which were confirmed to be functional using a qPCR melt curve analysis. For the in vivo gene expression analysis, n represented the number of mice, whereas in the in vitro experiments, n represented the number of culture dishes.

Transcriptome Analysis and Data Processing

The transcriptome analysis was conducted using a mouse Clariom S array (Thermo Fisher Scientific). The quantity and quality of RNA were assessed using microvolume spectrophotometry with the NanoDrop ND 1000 system (Thermo Fisher Scientific) and on chip capillary electrophoresis using a Bioanalyzer 2100 instrument (Agilent Technologies). All reactions and hybridizations were performed in accordance with the manufacturers' protocols. In brief, biotinylated single stranded complementary DNA was generated for hybridization using the GeneChip WT PLUS reagent kit (Thermo Fisher Scientific). The arrays were stained using GeneChip Fluidics Station 450, then scanned using the GeneChip scanner 3000 7G system (Thermo Fisher Scientific). The GeneChip Command Console Software ver.3.2 (Thermo Fisher Scientific) was used to convert the raw data of the image files into intensity data. The intensity data were processed to perform gene level normalization, quality control, and data analysis using the Transcriptome Analysis Console Software ver. 4.0.2 (Thermo Fisher Scientific).

Small Interfering RNA Transfection to Endothelial Cells

Human umbilical vein endothelial cells (HUVECs, CA20005N; TOYOBO) were purchased and cultured in VascuLife VEGF endothelial medium (LEL LL0003; Lifeline Cell Tech) at 37 °C in an atmosphere of 5% CO_2. HUVECs were used to investigate the potential inhibitory effect of AM2 on TGF β2 and TNF α mediated EndMT, which is mediated via Meox2 upregulation. HUVECs were transfected with small interfering RNA (siRNA) according to the manufacturer's protocol and as previously described.[38,39] In brief, the day before the experiments, OIR s were seeded at a density of 2.0×10^3 cells/well for 24 hours, then treated with a 1:1 mixture of 1 μM Meox2 siRNA oligos (target sequences: GCUUAAAACA AUUAGGAUC, GCAGUGAUGUUUAAUAAUA, UCAUGAUUUAUAGAGGGUU, and GAACUUGCUUUGAAUAAUC) in 100 μL of Accell siRNA delivery medium (GE Healthcare Dharmacon) and VEGF endothelial medium (VascuLife) (500 nM Meox2 siRNA). Cells in Accell siRNA delivery medium without siRNA treatment were used as the control. To confirm whether Meox2 siRNA was functional, we compared the expression of Meox2 using qPCR between the negative control siRNA (siRNA with a sequence that does not target any gene product) and Meox2 siRNA.

Induction of Endothelial to Mesenchymal Transition and the Measurement of NF κB Activation in Human Umbilical Vein Endothelial Cells

HUVECs transfected with Meox2 siRNA were used to investigate the potential inhibitory effect of AM2 on EndMT and nuclear factor kappa B (NF κB) activation, which are mediated via Meox2. For this experiment, the cells were pretreated with PBS or AM2 (10^{-7} mol/L) for 24 hours, followed by treatment with TGF β2 (5 ng/mL) and TNF α (10 ng/mL) for an additional 48 hours. The fluorescent immunostaining of HUVECs was performed using an anti vascular endothelial (VE) cadherin antibody (Abcam). The cells were also stained with phalloidin to visualize actin fibers. Positive areas were determined using the Hybrid Cell Count software after haze reduction (Keyence). For the NF κB activation experiment, the cells were pretreated with PBS or AM2 (10^{-7} mol/L) for 3 hours, followed by treatment with TNF α (10 ng/mL) for an additional 5 minutes. Whole cell extracts were prepared from HUVECs. NF κB p65 was analyzed using an enzyme linked immunosorbent assay (Abcam), which uses a tetramethylbenzidine colorimetric substrate to detect the total and phospho NF κB p65 attached to the consensus binding sites in a 96 well plate. Measurements were made based on the optical density 450 using a SpectraMax 190 microplate reader (Molecular Devices). Standard curves were derived using 4 parameter logistic regression. Relative expression values for each experimental sample were calculated from these curves. Every test was repeated at least 3 times.

Statistical Analysis

Statistical analyses other than the transcriptome analysis were performed using the GraphPad Prism 9.3.1 software (GraphPad). Differences were assessed using the Mann–Whitney *U*, 1 way analysis of variance with Kruskal–Wallis, 2 way analysis of variance with Kruskal–Wallis, or χ^2 test. $P < .05$ was considered statistically significant. Values are presented as the mean ± SEM.

Results

AM2 / Neonates Do Not Show Major Abnormalities in Retinal Angiogenesis

In the OIR model (Fig. 1A), neonates were exposed to 75% oxygen for 5 days, from P7 to P12. During this period (hyperoxic phase), the oxygen induced loss of retinal vessels (vaso obliteration) occurs. After the mice were returned to normoxic conditions (room air) for 5 days, from P12 to P17 (hypoxic phase), the hyperoxia induced vessel loss led to pathologic angiogenesis.

Our initial comparison of the developing mouse retinal vessels on P7 (physiological angiogenesis) in the lectin stained whole retinas between WT and AM2 / neonates showed that they were

counted. Scale bar 100 μm. (D) Bar graphs comparing CNV and fibrotic areas and macrophage invasion between AM2-/- and WT mice. AM2-/- mice had more enlarged CNV lesions with significantly exacerbated subretinal fibrosis and macrophage infiltration compared with WT mice. (E) Hematoxylin-eosin staining and immunostaining for α-SMA (diaminobenzidine) in the sections of retina 7 days after laser irradiation. Dotted circles show the LI-CNV lesions. Scale bar 100 μm. (F) Quantitative real-time PCR analysis of the gene expression related to angiogenesis, inflammation, oxidative stress, and fibrosis in the choroid 7 days after laser irradiation. Means of WT mice were assigned a value of 1. Bars are means ± SEM. *$P < .05$, **$P < .01$, and ****$P < .0001$. *P* values were calculated using the Mann Whitney *U* test (A, D, and F) and the 1-way analysis of variance with the Kruskal Wallis test (B). CGRP, calcitonin gene-related peptide; CLR, calcitonin receptor-like receptor; CTGF, connective tissue growth factor; FITC, fluorescein isothiocyanate; HE, hematoxylin-eosin; RAMP, receptor activity-modifying protein; α-SMA, α-smooth muscle actin; TGF, transforming growth factor; TNF, tumor necrosis factor; VEGF, vascular endothelial growth factor; VEGFR, vascular endothelial growth factor receptor.

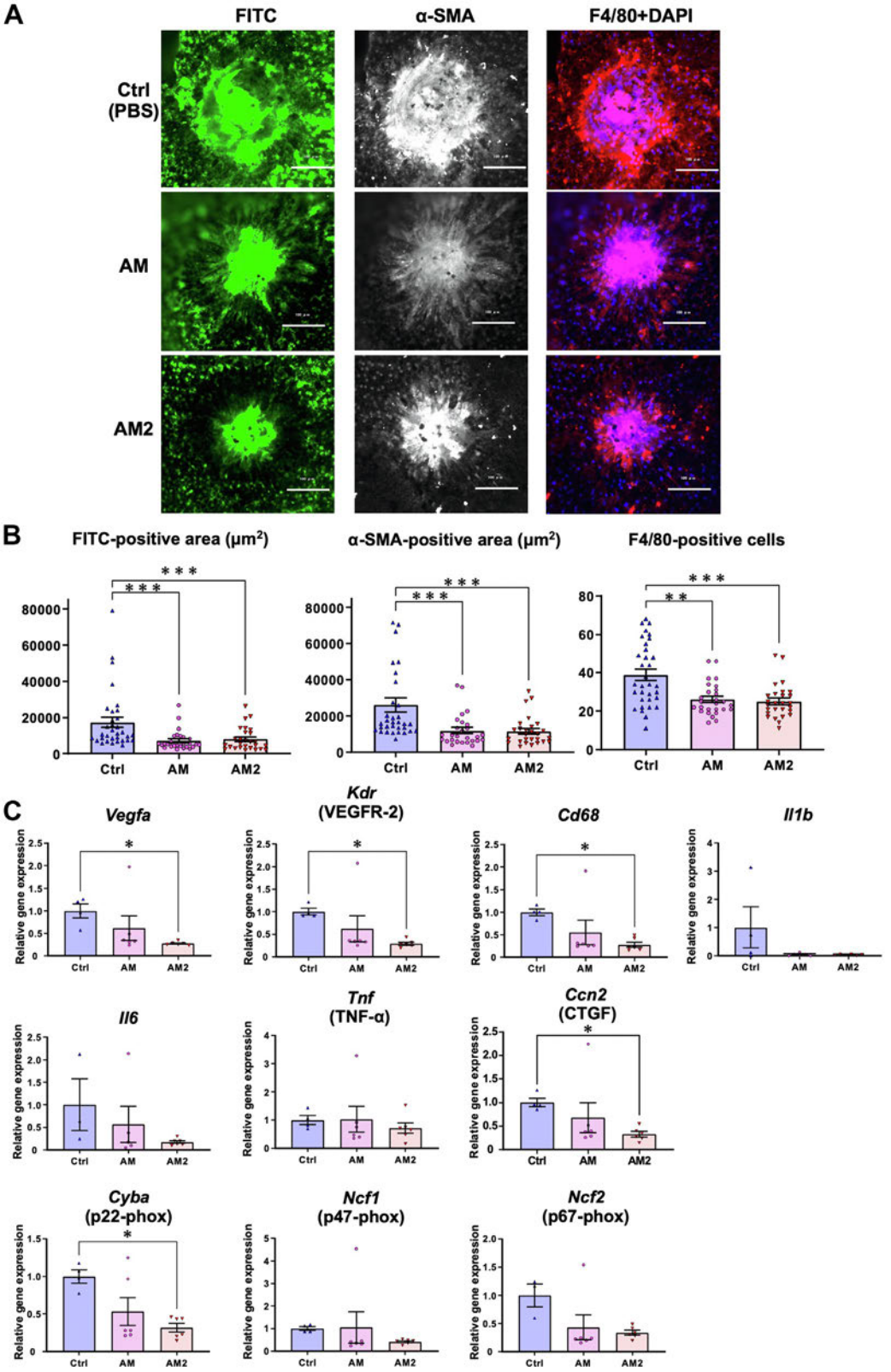

Figure 3.

Evaluation of laser-induced choroid neovascularization (LI-CNV) in systemic adrenomedullin 2 (AM2)- or AM-administered mice. (A) Comparison of LI-CNV among mice systemically administered phosphate-buffered saline (PBS), AM, or AM2. On day 7, after laser-induced injury to the Bruch membrane, choroidal flat mounts were prepared, the fluorescein isothiocyanate-positive CNV and αSMA-positive fibrotic areas were measured, and the number of F4/80-positive macrophages was counted. (B) Bar graphs comparing the CNV and fibrotic areas and macrophage invasion among PBS-, AM-, and AM2-administered mice. AM2 or AM treatment suppressed the extent of CNV, fibrosis, and macrophage invasion. (C) Quantitative real-time PCR analysis of the gene expression related to angiogenesis, inflammation, oxidative stress, and fibrosis in the choroid 7 days after laser irradiation. Means of PBS-administered control mice were assigned a value of 1. AM2 treatment suppressed the expression of *Vegfa, Kdr, Cd68, Ccn2, and Cyba.* Bars indicate the mean ± SEM. *$P < .05$, **$P < .01$, and ***$P < .001$. P values were calculated using the one-way analysis of variance with the Kruskal Wallis test (B and C). CTGF, connective tissue growth factor; FITC, fluorescein isothiocyanate; α-SMA, α-smooth muscle actin; TNF, tumor necrosis factor; VEGFR, vascular endothelial growth factor receptor.

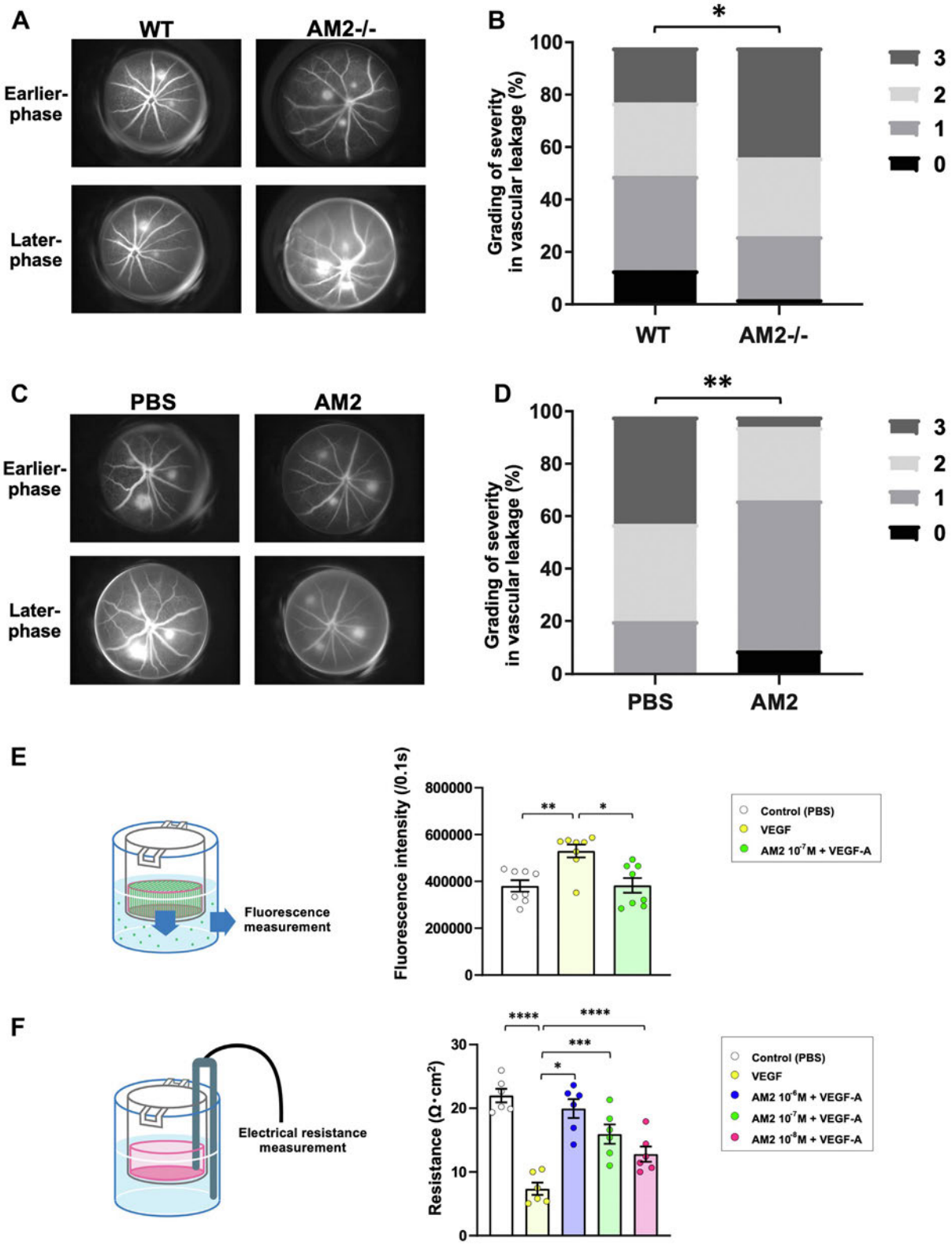

Figure 4.

Improvement of retinal vascular barrier function and suppression of vascular leakage from laser-induced choroid neovascularization (LI-CNV) by adrenomedullin 2 (AM2). (A) Representative photos of fluorescein angiography (FA) in wild-type (WT) and AM2-knockout (AM2-/-) mouse eyes 7 days after laser irradiation. Photos were taken at the earlier phase (2-3 minutes) and the later phase (5-6 minutes) after fluorescein injection. (B) Histogram showing the percentage of each CNV leakage grade in WT and AM2-/- mouse eyes. Vascular leakage was evaluated using the grading scheme outlined in the Materials and Methods section. Larger CNV lesions with greater leakage on FA developed in AM2-/-. (C) Representative FA of systemic phosphate-buffered saline (PBS)-administered and AM2-administered mouse eyes at the earlier and later phases after fluorescein injection. (D) Histogram showing the percentage of each CNV leakage grade in PBS- or AM2-administered mouse eyes. Smaller CNV lesions with lower leakage on FA developed in AM2-administered mice. Retinal vascular permeability was enhanced in AM2-/- mice, whereas it was decreased by AM2 treatment. Number of the laser spots; n 69 in both

elongating from the center of the retina toward the periphery in the superficial layer (Fig. 1B). The vascular progression did not differ between WT and AM2 / neonates (Fig. 1C). We also quantified the vascular density and branching in the area near the developing vascular front and found no significant differences between the 2 genotypes (Fig. 1D, E).

We then evaluated whether the relative ischemia induced by high concentrations of oxygen and subsequent normoxia evoked changes in pathologic retinal angiogenesis. In the OIR model, both WT and AM2 / neonates exposed to hyperoxia exhibited avascular areas in the central region of the retina on P12 (Fig. 1F), and no significant differences in the sizes of the avascular areas were detected between the 2 groups (Fig. 1G). An analysis of the P17 retinas revealed that the avascular areas were significantly reduced in AM2 / than in WT neonates. On the other hand, the formation of neovascular tufts generated by pathologic angiogenesis did not differ between AM2 / and WT neonates (Fig. 1H, I). These results are somewhat different from our previous study in heterozygous AM knockout (AM+/) mice, which showed a reduced avascular area and neovascular tuft formation.[22]

To examine the cause of the different results of the OIR model between AM+/ and AM2 / neonates, we examined the time course of the expression of AM and AM2 (Fig. 1J). The relative ischemia induced by OIR markedly increased AM expression on P17, whereas AM2 expression was decreased. This suggests that the significance of AM2 in retinal angiogenesis during the developmental stage of neonates may be relatively low compared with that of AM. In support of this idea, exogenous intravitreal administration of AM increased neovascular tuft formation, whereas that of AM2 did not (Supplementary Fig. S1A, B).

AM2 / Mice Show Exacerbated Laser Induced Choroidal Neovascularization, Fibrosis, and Inflammation

We next compared the distribution of the receptor components of AM2 between the retina and choroid. Peptides belonging to the calcitonin superfamily, including AM2, partially share their receptor system. One of the subisoforms of receptor activity modifying protein (RAMP) binds to calcitonin receptor like receptor (CLR), a 7 transmembrane G protein, in a one to one manner and subsequently functions as a receptor for these peptides. The real time qPCR analysis of the retina and choroid of 12 week old WT mice revealed that RAMP3 expression was equivalent in both the layers. In contrast, the expression of CLR, RAMP1, and RAMP2 was approximately 13 , 22 , and 35 fold higher, respectively, in the choroid than in the retina (Fig. 2A). Based on these results, we hypothesized that AM2 might be involved more in choroidal angiogenesis than in retinal angiogenesis.

To clarify the involvement of AM2 in pathologic choroidal angiogenesis, we next analyzed LI CNV, a model of nAMD. Following laser irradiation, the expression of RAMP2 and RAMP3 peaked on days 3 and 1, respectively, and then returned to basal levels. In addition, CLR expression gradually increased from day 1 to day 7 (Fig. 2B). The expression of the AM2 receptor system was elevated in the LI CNV model, suggesting the involvement of AM2 in this pathologic condition.

To investigate the significance of endogenous AM2 in the pathogenesis of LI CNV, laser irradiation was performed on AM2 / and WT mouse eyes, and choroidal flat mounts were generated 1 week after the procedure. As a result, AM2 / mice had significantly larger FITC and α SMA positive areas (CNV size and fibrosis, respectively) and a higher number of F4/80 positive cells around CNV lesions (inflammation) than had WT mice (Fig. 2C, D). We also examined the sections of the LI CNV lesions and found that AM2 / mice had larger lesions and more intense destruction of the laminar structure of the retina, and severe subretinal fibrosis (Fig. 2E). The examination of choroidal flat mounts 2 weeks after the laser irradiation yielded almost identical results (Supplementary Fig. S2A, B).

The expression of the genes involved in angiogenesis, inflammation, oxidative stress, and fibrosis in the choroid was also higher in AM2 / than in WT mice after 1 week of laser irradiation (Fig. 2F).

Exogenous AM2 Suppresses CNV Formation, Fibrosis, and Inflammation, and Suppresses the Expression of Associated Genes in the Choroid

Because endogenous AM2 deficiency exacerbated the pathology of LI CNV, we examined whether exogenous administration of AM2 could conversely ameliorate the pathology of LI CNV. We systemically administered AM or AM2 to WT mice using an osmotic pump and PBS as a control and compared their responses with those of laser irradiation after 1 week. Consistent with our previous reports and results,[31] systemic administration of AM reduced CNV formation, fibrosis, and inflammation (Fig. 3A, B). Systemic administration of AM2 improved each LI CNV score to the same extent as AM (Fig. 3A, B). We also examined the effects of local administration of AM or AM2 using intravitreal injection. Intravitreal administration in mice increased the CNV and fibrotic areas, even in the control PBS, owing to the puncture effect itself. However, intravitreal administration of AM or AM2 reduced CNV, fibrosis, and inflammation equally compared with those in the control (Supplementary Fig. S3A, B).

When gene expression related to angiogenesis, inflammation, oxidative stress, and fibrosis in the choroid of mice treated with LI CNV was examined by real time qPCR, we found that the expression of genes encoding VEGF A, VEGF receptor 2, CD68, connective tissue growth factor, and p22 phox was significantly decreased in mice treated with systemic administration of AM2 compared with that in the control (Fig. 3C).

AM2 Maintains the Barrier Function of Endothelial Cells and Inhibits Retinal Vascular Permeability

Another important pathology in nAMD is retinal edema caused by increased vascular permeability, which can lead to severe visual impairment when the edema extends to the macula.

WT and AM2-/- groups (B), and n 24 in the PBS group, and n 21 in the AM2 group (D). (E) Effects of 20-ng/mL VEGF-A and/or 10^{-7}-mol/L AM2 on transendothelial fluorescein isothiocyanate (FITC)-dextran permeability at 180 minutes. TR-iBRB cells were cultured on a semipermeable membrane until they formed a tight monolayer. Endothelial permeability was determined by measuring the passage of FITC-labeled dextran through the TR-iBRB monolayer. (F) Effects of 20-ng/mL VEGF-A and/or 10^{-8}- to 10^{-6}-mol/L AM2 on the transendothelial electrical resistance (TEER). TEER in the TR-iBRB cell monolayer was measured at 180 minutes using the Millicell-ERS2 Epithelial Volt/Ohm Meter system. The barrier function of retinal vascular endothelial cells was impaired by VEGF-A, whereas AM2 improved it. Bars indicate the mean ± SEM. *$P < .05$, **$P < .01$, ***$P < .001$, and ****$P < .0001$. *P* values were calculated using the $\chi 2$ test (B and D) and the 1-way analysis of variance with the Kruskal Wallis test (E and F). VEGF, vascular endothelial growth factor.

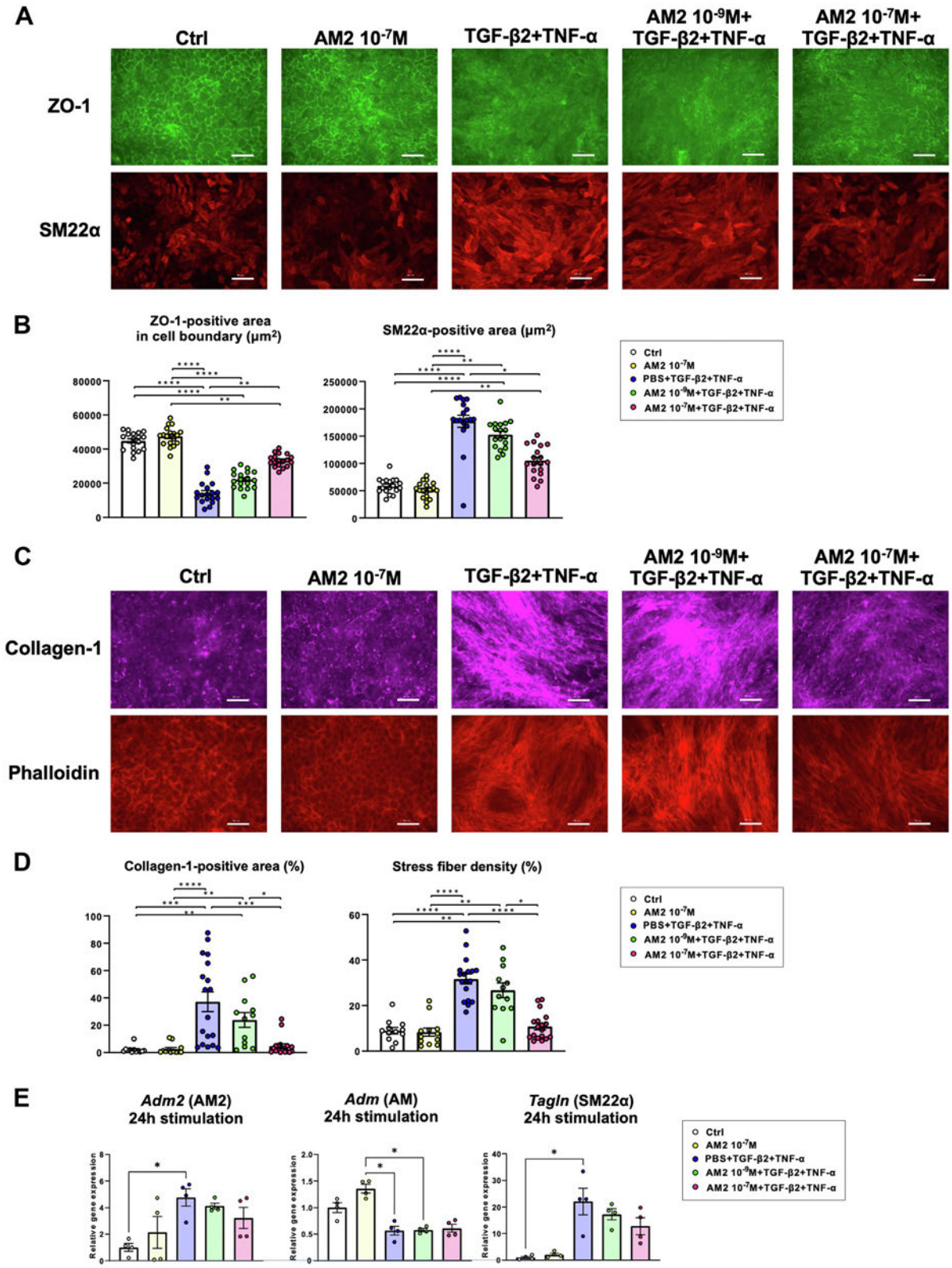

Figure 5.

Suppression of epithelial-to-mesenchymal transition (EMT) of cultured retinal pigment epithelial cells by adrenomedullin 2 (AM2). (A) Immunostaining for zonula occludens protein 1 (ZO-1) (upper panels) and SM22α (lower panels) in adult retinal pigment epithelial cell line 19 (ARPE-19) human retinal pigment epithelial cells. Cells were stimulated with transforming growth factor (TGF)-β2 (5 ng/mL) plus tumor necrosis factor (TNF)-α (10 ng/mL) for 48 hours to induce EMT. AM2 (10^{-9} or 10^{-7} mol/L) or phosphate-buffered saline (PBS) was added 24 hours before EMT induction. ZO-1 and SM22α were used as epithelial and mesenchymal markers, respectively. Scale bar 100 μm. (B) Bar graphs comparing the ZO-1- and SM22α-positive areas/field (magnification: ×20). For ZO-1, only the cell boundary region was measured. (C) ARPE-19 cells were immunostained for collagen 1 (upper panels) or stained with phalloidin (lower panels) to evaluate the extracellular matrix and the changes in the actin cytoskeleton, respectively. Scale bar 100

Therefore, we proceeded to examine whether AM2 functions to stabilize the blood retina barrier and suppress retinal vascular leakage. We analyzed the leakage from the LI CNV lesions by performing FA on day 7 after the laser irradiation. Figure 5 shows typical fluorescence images obtained at earlier (2 3 minutes) and later (5 6 minutes) times after fluorescein injection. By using FA, we found that AM2 / mice developed larger angiographic leak ages from the CNV lesions than WT mice (Fig. 4A). In particular, the numbers of grade 3 (pathologically significant leakage) le sions were approximately 2 fold higher in AM2 / than in WT mice (Fig. 4B). Next, we examined the angiogenic leakage from the LI CNV lesion in WT mice treated systemically with AM2. AM2 treated mice showed significantly reduced angiogenic leakage compared with the control, and grade 3 lesions were almost ab sent (Fig. 4C, D). These results indicate that AM2 is effective in ameliorating the pathology of LI CNV by inhibiting vascular permeability.

From the observed effects of AM2, we speculated that AM2 could suppress VEGF A evoked retinal vascular hyperpermeability. To test this hypothesis, we analyzed transendothelial permeability using TR iBRB cells. TEFP was determined by measuring the pas sage of FITC labeled dextran from the upper to the lower compartment through a monolayer of TR iBRB cells. Our findings indicated that VEGF A significantly increased endothelial perme ability and that the coadministration of AM2 suppressed this effect (Fig. 4E). VEGF A also significantly reduced the TEER, and AM2 dose dependently inhibited the reduction of TEER elicited by VEGF A (Fig. 4F). The VEGF A induced disruption of endothelial barrier function was therefore ameliorated by AM2.

The Epithelial to Mesenchymal Transition of Retinal Pigment Epithelial Cells Is Suppressed by AM2

The in vivo study revealed the protective effect of the AM RAMP2 system against subretinal fibrosis. Recently, there has been growing interest in EMT as the mechanism involved in various fibrosis related diseases, including subretinal fibrosis.[40,41] Among the retinal cell components, retinal pigment epithelial cells are most susceptible to EMT. We, therefore, evaluated EMT using ARPE 19 cells. To induce EMT, ARPE 19 cells were stimu lated with TGF β2 plus TNF α for 48 hours. Immunostaining was performed to assess the expression of ZO 1, an epithelial cell marker detected in the cell membrane, and SM22α, a cytosolic marker of mesenchymal cells (Fig. 5A). We found that stimulation with TGF β2 plus TNF α resulted in the downregulation of ZO 1 and upregulation of SM22α, which suggested the induction of EMT (Fig. 5B). Using this protocol, the cells were pretreated for 24 hours with or without AM2 (10^{-9} M or 10^{-7} M) before the stimu lation. AM2 (10^{-7} M) significantly upregulated ZO 1 and down regulated SM22α, thereby preventing the effect of TGF β2 plus TNF α (Fig. 5A, B). The stimulation of ARPE 19 cells with TGF β2 and TNF α for 24 hours produced similar results (Supplementary Fig. S4A, B). Furthermore, collagen positive areas (indicating the accumulation of the extracellular matrix) and phalloidin positive actin filament formation (indicating myofibroblast like changes in ARPE 19 cells) were enhanced by TGF β2 plus TNF α stimulation, which indicated that EMT was certainly induced. Those changes were also prevented by AM2 (10^{-7} M) (Fig. 5C, D). The suppression of EMT may explain some of the protective effects of AM2 against subretinal fibrosis.

A gene expression analysis showed that the stimulation of ARPE 19 cells with TGF β2 plus TNF α significantly enhanced the expression of AM2 (Fig. 5E). In contrast, AM expression was reduced by the stimulation with TGF β2 plus TNF α. The gene expression of SM22α was significantly enhanced when the ARPE 19 cells were stimulated with TGF β2 and TNF α, but AM2 elimi nated this difference, supporting the phenomenon that EMT was suppressed by AM2.

Transcriptome Analysis Identifies Meox2 as a Candidate Factor That Mediates the Ameliorative Effects of AM2 on the Pathogenesis of LI CNV

To further explore the mechanisms underlying the ameliora tive effects of AM2 on the pathogenesis of LI CNV, we compre hensively analyzed gene expression in WT mice treated systemically with AM, AM2, or PBS by a transcriptome analysis of LI CNV samples 1 week after the laser irradiation (Fig. 6A D). A transcriptome analysis identified 113 and 82 genes in the AM and AM2 treated groups compared with the control PBS treated group, respectively, with expression levels that were signifi cantly changed by >2 fold or <0.5 fold. These genes included 15 genes that were commonly altered in the AM and AM2 treated groups (Fig. 6E and Table 2), whereas 63 genes were differen tially altered between the groups.

Factors commonly altered in the AM and AM2 groups are likely important in ameliorating LI CNV. Among them, we focused on the transcription factor Meox2, which is commonly upregulated in both groups. In the LI CNV samples of the WT mice, the expression of Meox2 was downregulated the day after laser irradiation. However, its expression recovered to the preirradiation level by day 7 (Fig. 6F). The expression of Meox2 in day 1 LI CNV samples was confirmed by real time qPCR, which showed that it was significantly decreased in AM2 / mice compared with that in WT mice (Fig. 6G) and significantly increased in AM2 treated mice compared with that in the control PBS treated mice (Fig. 6H). We also examined immunohistochemistry in sections of the LI CNV samples and confirmed that Meox2 expression was reduced in AM2 / mice (Fig. 6I). Real time qPCR further showed that the upregulation and downregulation of a series of genes related to inflammation, fibrosis, and angiogenesis were opposite between mice treated with exogenous AM2 and AM2 / (Supplementary Fig. S5A, B).

On the other hand, in the transcriptome analysis, AM2 administration did not cause significant changes in the expression of pericyte markers (Table 3).

AM2 Suppresses Endothelial to Mesenchymal Transition and NF κB Activation in Endothelial Cells via Meox2

In addition to EMT, EndMT also plays an important role in the pathology of nAMD. We analyzed the role of AM2 in the regulation of EndMT and the involvement of Meox2 in this process. Meox2 siRNA was transfected into HUVECs, and qPCR confirmed that the expression of Meox2 gene was reduced to approximately half that

μm. (D) Bar graphs comparing the percentages of collagen 1 immunostaining positive area and phalloidin-positive stress fiber density. EMT induced by TGF-β2 plus TNF-α was canceled by AM2. (E) Quantitative real-time PCR analysis of the gene expression in ARPE-19 cells. Cells were stimulated with TGF-β2 plus TNF-α for 24 hours to induce EMT. AM2 or PBS was added 24 hours before EMT induction. Bars indicate the mean ± SEM. *$P < .05$, **$P < .01$, ***$P < .001$, and ****$P < .0001$. P values were calculated using the 1-way analysis of variance with the Kruskal Wallis test (B, D, and E). SM22α, smooth muscle 22α.

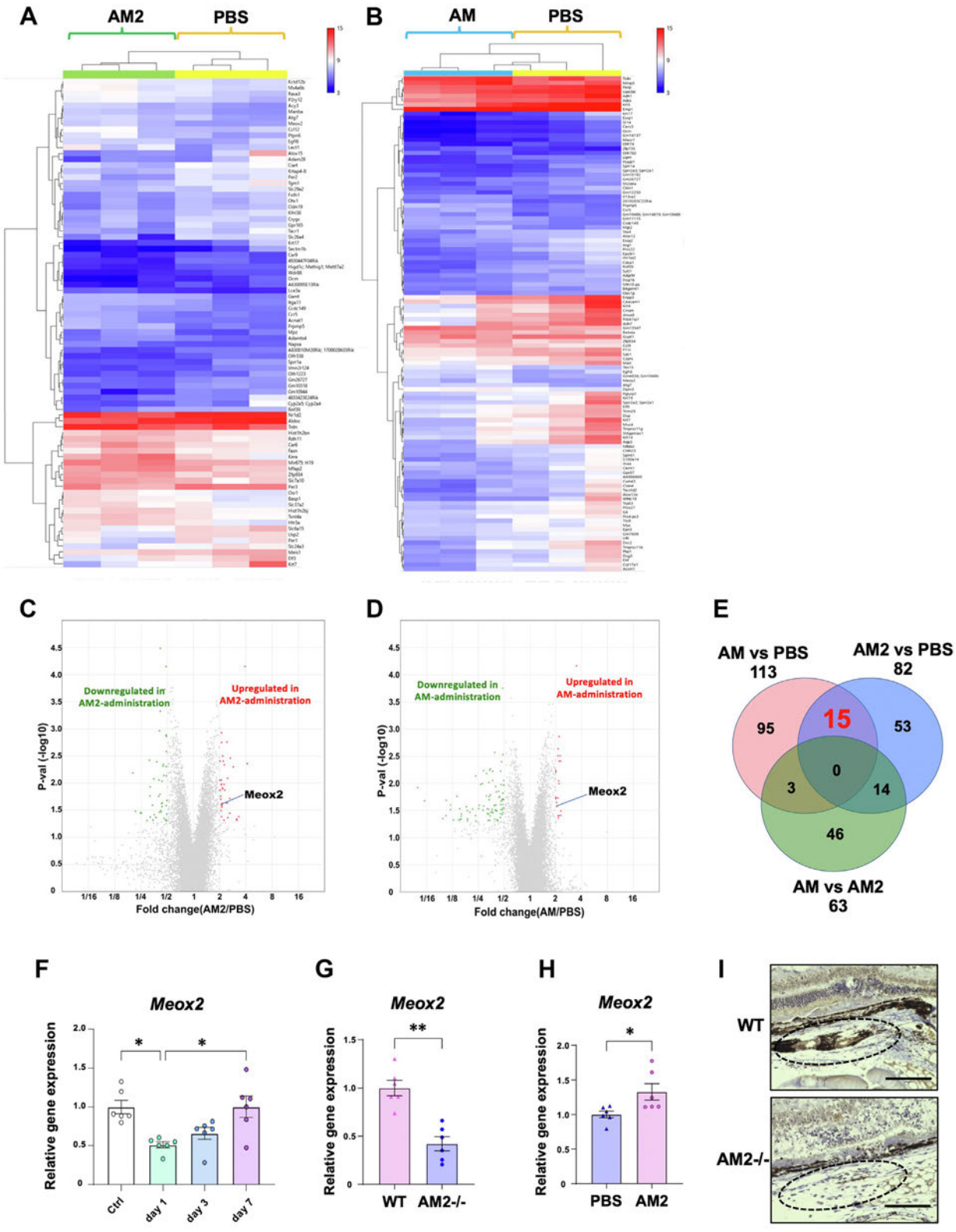

Figure 6.

Candidate genes identified by transcriptome analysis that are associated with the suppressive effects of adrenomedullin (AM) and AM2 on laser-induced choroid neovascularization (LI-CNV). (A-D) Hierarchical clustering analysis (A and B) and volcano plot analysis (C and D) of the differentially expressed genes in 1-week LI-CNV samples. Comparison between AM2- and phosphate-buffered saline (PBS)-administered mice (A and C) and comparison between AM- and PBS-administered mice (B and D) are shown (n 3 in each). Red spots represent the upregulated genes, and the green ones represent the downregulated genes, with the fold change on the X-axis and the *P* value on the Y-axis. The gray-colored region represents the nonsignificantly differentially expressed genes (C and D). (E) Venn diagram showing the number of differentially expressed genes per comparison. Transcriptome analysis identified 15 candidate genes associated with the suppressive effects of AM2 and AM in common,

Table 2
Fifteen genes commonly and significantly upregulated or downregulated by AM2 or AM administration in the laser-irradiated choroid (vs control)

Gene	NCBI reference sequence	Description	Fold change (AM2 vs control)	*P* value	Fold change (AM vs control)	*P* value	ID
Prpmp5	NM_001024705	proline-rich protein MP5	3.91	.0000699	3.49	.0000677	TC0600003281.mm.2
Ccr5	NM_009917	chemokine (C-C motif) receptor 5	2.66	.0035	2.20	.0014	TC0900001675.mm.2
Zfp934	NM_001162911	zinc finger protein 934	2.20	.0039	2.01	.019	TC1300002768.mm.2
Gm26727	ENSMUST00000180773	predicted gene, 26727 [Source:MGI Symbol;Acc:MGI:5477221]	0.46	.0072	0.49	.0089	TC0200003685.mm.2
Ccdc149	NM_001256059	coiled-coil domain containing 149	2.03	.0135	2.12	.0187	TC0500002410.mm.2
Krt17	NM_010663	keratin 17	0.32	.0172	0.33	.0096	TC1100003763.mm.2
Meox2	NM_008584	mesenchyme homeobox 2	2.09	.0248	2.05	.0265	TC1200000331.mm.2
Elf3	NM_001163131	E74-like factor 3	0.34	.0255	0.28	.0101	TC0100003123.mm.2
Rnf39	NM_001099632	ring finger protein 39	0.40	.0344	0.23	.0073	TC1700000750.mm.2
Krt7	NM_033073	keratin 7	0.25	.0355	0.12	.0303	TC1500001073.mm.2
Trdn	NM_029726	triadin	3.31	.0415	2.29	.0389	TC1000000286.mm.2
Egfl6	NM_019397	EGF-like domain, multiple 6	2.11	.0416	2.20	.0391	TC0X00003349.mm.2
Sprr1a	NM_009264	small proline-rich protein 1A	0.32	.0419	0.27	.0104	TC0300002393.mm.2
Atg7	NM_001253717	autophagy related 7	2.48	.0434	2.30	.0322	TC0600001271.mm.2
Ocm	NM_033039	oncomodulin	0.49	.0493	0.45	.0245	TC0500003569.mm.2

Abbreviations: AM, adrenomedullin; AM2, adrenomedullin 2.

of the control (Fig. 7A). In cultured HUVECs, stimulation with TGF β2 plus TNF α reduced the distribution of VE cadherin at the cellular membrane and increased the formation of actin stress fiber, indicating that EndMT had occurred (Fig. 7B). Pretreating the cells with AM2 antagonized the effect of the stimulation, reversing the loss of VE cadherin from the cellular membrane (Fig. 7C, left) and the formation of stress fibers (Fig. 7C, right). Thus, AM2 can suppress EndMT caused by stimulation with TGF β2 plus TNF α. On the other hand, when Meox2 gene was knocked down prior to AM2 treatment, the inhibitory effect of AM2 on EndMT tended to be canceled.

NF κB orchestrates the transcription of a wide range of inflammation related molecules. Meox2 has been reported to regulate NF κB and inflammatory responses in vascular endothelial cells.[25] Therefore, we examined the involvement of Meox2 in the regulation of NF κB activity by AM2. We evaluated NF κB activation using enzyme linked immunosorbent assays to measure the levels of phospho NF κB p65 in whole cell extracts (Fig. 7D). We found that TNF α elevated the activation of the NF κB pathway but that the pretreatment of AM2 suppressed this effect. This effect of AM2 tended to be canceled by the knockdown of Meox2 gene. AM2, therefore, exerts an inhibitory effect on EndMT and NF κB activation in endothelial cells, which may be partially mediated by Meox2.

Discussion

This study analyzed the relationship between AM2 and ocular lesions in the OIR and LI CNV models in mice. The results showed that AM2 is not involved in physiological retinal angiogenesis during the developmental stage of neonates, nor is it involved in pathologic retinal angiogenesis in response to ischemia. The deletion of endogenous AM2, however, resulted in the enhancement of pathologic, hyperpermeable CNV and increased subretinal fibrosis and inflammation, resulting in the deterioration of the pathologic state of nAMD. In contrast, exogenous administration of AM2 ameliorated the LI CNV lesions and suppressed the expression of factors related to pathologic angiogenesis, inflammation, fibrosis, and oxidative stress. AM2 inhibited the progression of subretinal fibrosis by suppressing the EMT of retinal pigment epithelial cells and EndMT of endothelial cells. Transcriptome and gene knockdown analyses revealed that AM2 ameliorated each pathologic state through the upregulation of Meox2, a transcription factor that suppresses inflammation and fibrosis.

AM2, together with AM and calcitonin gene related peptide (CGRP), is a peptide belonging to the calcitonin superfamily. They share structural similarities in having an intramolecular ring structure consisting of disulfide bonds and amidation at the C terminus, and functional similarities as vasodilators.[42-44] AM, CGRP, and AM2 are ligands of the G protein coupled receptor CLR. The binding of RAMPs to CLR modulates its affinity to these ligands and regulates its function.[45] There are many clinical reports of peptides belonging to the calcitonin superfamily being significant in ocular diseases. CGRP is abundant in tear fluid, and its concentration is reduced in severely dry eyes.[46] The levels of AM in the vitreous and aqueous humor are elevated in human diabetic retinopathy, primary open angle glaucoma, and nAMD.[47-50] In relation to human genetic variations, AM binds to complement factor H.[51] An intronic and common variant in the complement factor H gene is strongly associated with human nAMD; in individuals homozygous for the risk allele, the likelihood of nAMD is increased by a factor of 7.4.[52,53] Although the importance of AM and CGRP in various ocular diseases has been reported, the significance of AM2 remains unclear. Therefore, we generated AM2 / mice to investigate the pathophysiological roles of AM2 in ocular diseases.

including Meox2. (F) Quantitative real-time PCR analysis of the expression of Meox2 in the choroid of untreated control wild-type (WT) mice and WT mice on days 1, 3, and 7 after laser irradiation. Means of control mice were assigned a value of 1. Meox2 expression was transiently decreased after laser irradiation but gradually returned to its baseline level by day 7. (G and H) Quantitative real-time PCR analysis of Meox2 in the choroid of WT and AM2-knockout (AM2-/-) mice (G) and systemic PBS- and AM2-administered mice (H) 1 day after laser irradiation. Means of WT mice (G) or PBS-administered mice (H) were assigned a value of 1. Meox2 expression was decreased in AM2-/- mice but increased by exogenous administration of AM2. (I) Immunostaining for Meox2 (diaminobenzidine) in the retina sections 1 day after laser irradiation. Dotted circles show the LI-CNV lesions. Scale bar 100 μm. Data are expressed as the mean ± SEM. *$P < .05$ and **$P < .01$. *P* values were calculated using the 1-way analysis of variance with the Kruskal Wallis test (F) and the Mann Whitney *U* test (G and H).

Table 3
Change in expression of pericyte markers by AM2 administration in the laser-irradiated choroid (vs control)

Gene	NCBI reference sequence	Description	Fold change (AM2 vs control)	*P* value	ID
Abcc9	NM_001044720; NM_011511; NM_021041; NM_021042	ATP-binding cassette, subfamily C (CFTR/MRP), member 9	1.02	.859	TC0600003379.mm.2
Anpep	NM_008486	alanyl (membrane) aminopeptidase	0.98	.798	TC0700003570.mm.2
Cd248	NM_054042	CD248 antigen, endosialin	1.08	.670	TC1900000055.mm.2
Cspg4	NM_139001	chondroitin sulfate proteoglycan 4	1.12	.731	TC0900000686.mm.2
Des	NM_010043	desmin	0.85	.643	TC0100000657.mm.2
Dlk1	NM_001190703; NM_001190704; NM_001190705; NM_010052	delta-like 1 homolog (*Drosophila*)	1.37	.059	TC1200001125.mm.2
Kcnj8	NM_008428	potassium inwardly rectifying channel, subfamily J, member 8	0.93	.273	TC0600003378.mm.2
Mcam	NM_023061	melanoma cell adhesion molecule	1.77	.427	TC0900000500.mm.2
Ninj1	NM_013610	ninjurin 1	1.14	.428	TC1300000560.mm.2
Pdgfrb	NM_001146268; NM_008809	Platelet-derived growth factor receptor, beta polypeptide	1.12	.492	TC1800000623.mm.2
Rgs5	NM_009063	regulator of G-protein signaling 5	0.99	.929	TC0100001560.mm.2

Abbreviation: AM2, adrenomedullin 2.

Our study using CGRP homozygous knockout mice (CGRP /) showed no difference in physiological or pathologic retinal angiogenesis in neonates compared with WT mice.[28] Among the subisoforms of RAMPs, CGRP has the strongest affinity to RAMP1. Therefore, the CGRP RAMP1 system is not greatly involved in retinal angiogenesis. In contrast, homozygous knockout mice of either AM (AM /) or RAMP2 (RAMP2 /) are embryonically lethal because of abnormal vascular development,[54,55] indicating that the AM RAMP2 system is essential for normal vascular development. The observation of retinal vascular development during the early stage of neonatal development (P6) using drug inducible vascular endothelial cell specific RAMP2 knockout (DI E RAMP2 /) mice previously revealed an abnormal retinal vascular pattern in which vascular progression regressed while vascular density increased.[22] In the OIR model, neovascular tuft formation was suppressed in AM+/ mice and in mice treated with intravitreal injection of neutralizing antibodies against AM,[22] suggesting that endogenous AM is also responsible for pathologic retinal angiogenesis during ischemia.

The major difference between AM and AM2 is that AM2 / mice were born normally and could reach adulthood. This study also revealed no changes in physiological retinal angiogenesis in AM2 / compared with WT mice. Neovascular tuft formation in the OIR model was also unchanged in AM2 / mice. Although exogenous administration of AM increased neovascular tuft formation, AM2 did not alter it. In the OIR model, AM expression was markedly upregulated compared with that in normoxia, whereas AM2 expression was downregulated. It has been reported that AM2, like AM, promotes angiogenesis in several organs and tissues.[56,57] However, this study revealed that AM2 is less involved in physiological and pathologic retinal angiogenesis during neonatal development.

We further compared the gene expression of the AM2 receptor system in the retina and choroid and found that CLR, RAMP1, and RAMP2 are abundant in the choroid. Furthermore, the expression of CLR increased with time after laser irradiation. Therefore, we speculated that AM2 is more critical in choroidal angiogenesis than in retinal angiogenesis. To confirm this hypothesis, we examined the significance of AM2 in the LI CNV model. As expected, LI CNV lesions were exacerbated in AM2 / than in WT mice; conversely, they were ameliorated when AM2 was exogenously administered.

We, and other groups, have previously reported that AM and CGRP work to improve the pathogenesis of LI CNV based on studies using genetically engineered mice. We found that LI CNV lesions are exacerbated in CGRP / than in WT mice.[28] Endogenous CGRP suppresses the production of TNF α from macrophages and prevents the breakdown of intercellular tight junction structures in retinal pigment epithelial cells. Yuda et al[58] reported that LI CNV lesions are exacerbated in AM+/ mice. Endogenous AM suppresses macrophage infiltration and inflammation induced pathologic angiogenesis by inhibiting the production of monocyte chemoattractant protein 1 from retinal pigment epithelial cells. We found that LI CNV lesions are also exacerbated in RAMP2+/ mice.[31] The AM RAMP2 system suppresses the EMT of retinal pigment epithelial cells and subretinal fibrosis by inhibiting the TGF β RhoA ROCK1 CXCR4 pathway.

In this study, the suppressive effects of AM2 on LI CNV expansion, subretinal fibrosis, and inflammation were similar to those of AM and CGRP. AM2 also suppressed vascular permeability from the LI CNV lesions. Thus, AM2 may be involved in maintaining the barrier function of vascular endothelial and retinal pigment epithelial cells. In the pathogenesis of nAMD, preventing the expansion of CNV lesions and reducing edema and hemorrhages by making the vasculature stable are crucial for maintaining retinal function.

Another distinctive finding about AM2 was that the genes related to inflammation and fibrosis were significantly upregulated in AM2 / mice and downregulated in AM2 treated mice 1 day after laser irradiation. Therefore, AM2 may play an important role in the acute phase response to tissue injury. In support of this, in vitro experiments using ARPE 19 cells showed that AM2 expression was significantly enhanced 24 hours after EMT induction. AM2 also exerted an inhibitory effect on the EMT of ARPE 19 cells and the EndMT of HUVECs. In the eye, both EMT and EndMT play critical roles in the pathogenesis of subretinal fibrosis, the end stage of nAMD that leads to profound and permanent vision loss.[59] Predominant in subretinal fibrotic lesions are matrix producing mesenchymal cells that originate from the retinal pigment epithelium and choroidal endothelial cells through EMT and EndMT, respectively. TGF β is thought to be a key cytokine orchestrating both EMT and EndMT, and TNF α augments TGF β signaling.[60,61] Because the differential contribution of EMT and EndMT to the mesenchymal cell population in subretinal fibrosis and the possible synergistic effects of EMT and EndMT have not yet been clarified, it remains unclear what AM2 contributes to primarily. The inhibition of EMT and EndMT has been investigated mainly in cell cultures in vitro, and there are currently few drug candidates that have advanced to the

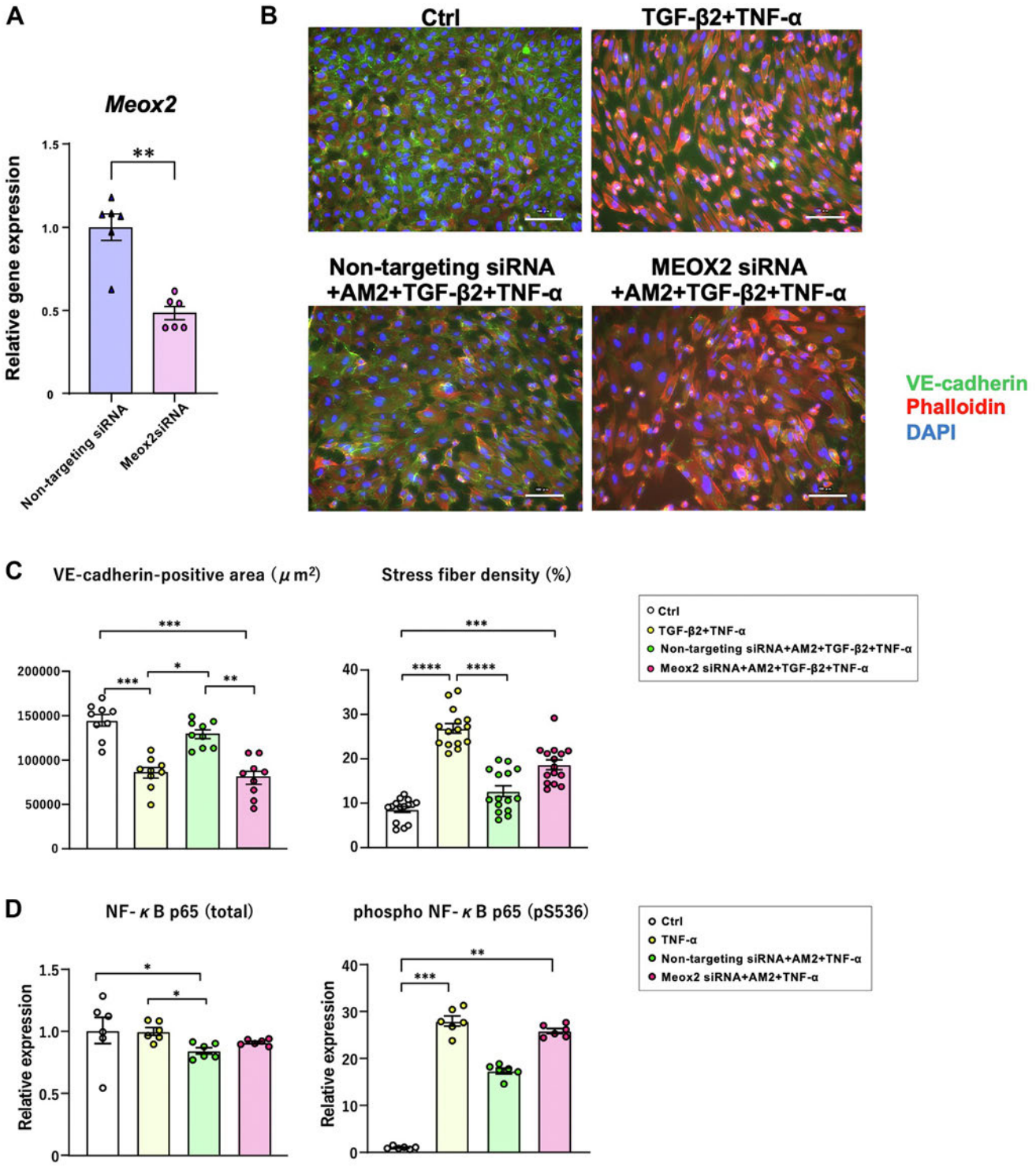

Figure 7.

Cancelation of the suppressive effects of adrenomedullin 2 (AM2) on endothelial-to-mesenchymal transition (EndMT) and nuclear factor kappa B (NF-κB) activation in endothelial cells by Meox2 gene knockdown. (A) Quantitative real-time PCR analysis of Meox2 in the human umbilical vein endothelial cells (HUVECs) transfected with control nontargeting small interfering RNA (siRNA) or Meox2 siRNA. Mean of the control was assigned a value of 1. (B) Immunostaining for vascular endothelial (VE)-cadherin and phalloidin staining in HUVECs. After the transfection of Meox2 siRNA or nontargeting control siRNA, the cells were stimulated with transforming growth factor (TGF)-β2 (5 ng/mL) plus tumor necrosis factor (TNF)-α (10 ng/mL) for 48 hours to induce EndMT. AM2 (10^{-7} mol/L) or phosphate-buffered saline (PBS) was added 24 hours before EndMT induction. Green, VE-cadherin; red, phalloidin; blue, DAPI. Scale bar 100 μm. (C) Bar graphs showing the VE-cadherin-positive areas/field (magnification: ×20) and the percentage of phalloidin-positive stress fiber density. For VE-cadherin, only the cell boundary region was measured. EndMT induced by TGF-β2 plus TNF-α was suppressed by AM2, but the effect tended to be canceled by Meox2 knockdown. (D) Quantification using enzyme-linked immunosorbent assay of NF-κB p65 and phospho-NF-κB p65 (Ser 536) in whole-cell extracts from HUVECs. The cells were pretreated first with AM2 (10^{-7} mol/L) or PBS for 3 hours and then with TNF-α (10 ng/mL) for 5 minutes. Mean of the control PBS group was assigned a value of 1. NF-κB activation caused by TNF-α (10 ng/mL) was suppressed by AM2. However, it tended to be canceled by Meox2 knockdown. Data are expressed as the mean ± SEM. *$P < .05$, **$P < .01$, ***$P < .001$, and ****$P < .0001$. P values were calculated using the Mann Whitney U test (A) and the 1-way analysis of variance with the Kruskal Wallis test (C and D).

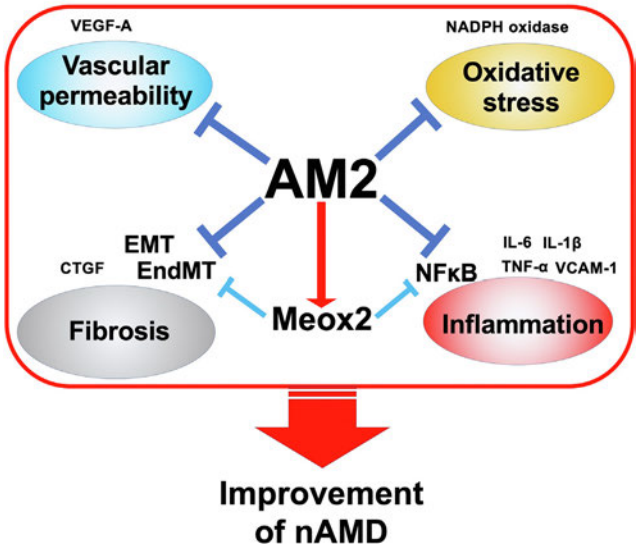

Figure 8.
Schematic review of the pathophysiological roles of adrenomedullin 2 (AM2) in neovascular age-related macular degeneration (nAMD). AM2 suppresses choroidal pathologic angiogenesis in nAMD, as well as vascular permeability, retinal edema, and inflammation. It also inhibits EMT and EndMT and suppresses the progression of subretinal fibrosis. The protective effects of AM2 are rapidly exerted via the upregulation of Meox2, which contributes to the quiescence of inflammation and fibrosis. CTGF, connective tissue growth factor; EMT, epithelial-to-mesenchymal transition; EndMT, endothelial-to-mesenchymal transition; IL, interleukin; NADPH, nicotinamide adenine dinucleotide phosphate; NF-κB, nuclear factor kappa B; TNF, tumor necrosis factor; VCAM-1, vascular cell adhesion molecule 1; VEGF, vascular endothelial growth factor.

preclinical stage of nAMD.[59] The finding that AM2 inhibits both EMT and EndMT is highly remarkable from a therapeutic perspective. Luo et al[62] identified choroidal pericytes as another source of myofibroblasts in the LI CNV model and found that choroidal pericytes express extracellular matrix components and participate in the formation of subretinal fibers.[63] In our transcriptome analysis, the expression of pericyte markers was not significantly altered by AM2 administration, suggesting that the effect on pericyte myofibroblast transition is not much involved in the ameliorative effect of AM2 on subretinal fibrosis.

Furthermore, we performed transcriptome analyses to explore novel mechanisms responsible for the ameliorative effects of AM2 on the pathogenesis of LI CNV. Meox2 is a vertebrate homeobox containing transcription factor originally cloned from mice (Mox 2) or rats (growth arrest homeobox).[64,65] Among the candidate genes in the transcriptome analyses, we focused on Meox2 as it is a transcription factor and would, therefore, be induced early after the laser induced tissue injury. Previous studies have reported that Meox2 is abundant in the cardiovascular system.[65,66] Meox2 has further been reported to be associated with angiogenesis, fibrosis, and inflammation.[23-26] Recently, Buchanan et al[67] reported that transcriptional profiling in DBA/2J mice, a widely used mouse model for glaucoma, could be used to detect early gene expression changes in response to increased intraocular pressure. They showed that Meox2 controls intraocular pressure dependent vascular remodeling and neuroinflammation to promote axon survival. Our data are consistent with those of previous studies that identified Meox2 as a transcription factor, the expression of which is induced early in response to tissue injuries and is vital for tissue repair.[24,68] As for its beneficial effects, Meox2 inhibits EMT and NF κB activation.[23,25] We found that the AM2 mediated suppression of EndMT and NF κB in endothelial cells is partially mediated by Meox2. Therefore, the protective effects of AM2 on the pathogenesis of LI CNV are partly mediated through Meox2 upregulation.

Figure 8 summarizes the pathophysiological roles of AM2 in ocular neovascular diseases. AM2 suppresses pathologic CNV in nAMD, vascular permeability, retinal edema, and inflammation. It also inhibits EMT and EndMT and suppresses the progression of subretinal fibrosis. The protective effects of AM2 are rapidly exerted via the upregulation of Meox2, which contributes to the quiescence of inflammation and fibrosis. Currently, nAMD is one of the leading causes of blindness in developed countries. Therefore, it is imperative to elucidate its precise pathogenesis.[69] Given our results and those of previous studies, AM2 may be further assessed as a novel therapeutic target for ocular neovascular diseases, especially nAMD.

Author Contributions

S.K. performed the experiments and wrote the manuscript. Y.M., K.H., A.I., and Y. Iesato analyzed the OIR and LI CNV models. T. Sakurai and A.K. generated genetically engineered mice. M.T. performed cellular experiments. Y. Ichikawa Shindo and H.K. performed histologic analyses. Y.Zhao, Y.Zhang, Q.G., P.L., and N.O. performed gene expression analyses. T.M. and T. Shindo planned the experiments and supervised the manuscript. All authors have read and approved the final paper.

Data Availability

Some or all data generated or analyzed during this study are included in this published article or supplementary data linked to this article.

Funding

This study was supported by Grants in Aid for Scientific Research (KAKENHI) to T. Shindo and K.H.; a grant from The Foundation for Eye Diseases in the Elderly to T. Shindo; grants from The Naito Foundation, The Takeda Science Foundation, The Mochida Memorial Foundation for Medical and Pharmaceutical Research, The Nakatomi Foundation, and The NOVARTIS Foundation (Japan) for the Promotion of Science to M.T.; and The Japanese Retina and Vitreous Society Basic Research Grant Program 2021 to S.K.

Declaration of Competing Interest

The authors declare no conflicts of interest.

Ethics Approval and Consent to Participate

All animal handling procedures were performed in accordance with the protocol approved by the Ethics Committee of Shinshu University School of Medicine. All experiments were performed in accordance with the Association for Research in Vision and Ophthalmology's Statement for the Use of Animals in Ophthalmic and Vision Research and our institutional guidelines.

Supplementary Material

The online version contains supplementary material available at https://doi.org/10.1016/j.labinv.2022.100038.

References

1. Nowak-Sliwinska P, Alitalo K, Allen E, et al. Consensus guidelines for the use and interpretation of angiogenesis assays. *Angiogenesis*. 2018;21(3):425 532. https://doi.org/10.1007/s10456-018-9613-x
2. Tan W, Zou J, Yoshida S, Jiang B, Zhou Y. The role of inflammation in age-related macular degeneration. *Int J Biol Sci*. 2020;16(15):2989 3001. https://doi.org/10.7150/ijbs.49890
3. Ardeljan D, Chan CC. Aging is not a disease: distinguishing age-related macular degeneration from aging. *Prog Retin Eye Res*. 2013;37:68 89. https://doi.org/10.1016/j.preteyeres.2013.07.003
4. Campochiaro PA. Molecular pathogenesis of retinal and choroidal vascular diseases. *Prog Retin Eye Res*. 2015;49:67 81. https://doi.org/10.1016/j.preteyeres.2015.06.002
5. Campochiaro PA. Ocular neovascularization. *J Mol Med (Berl)*. 2013;91(3): 311 321. https://doi.org/10.1007/s00109-013-0993-5
6. Mitchell P, Liew G, Gopinath B, Wong TY. Age-related macular degeneration. *Lancet*. 2018;392(10153):1147 1159. https://doi.org/10.1016/s0140-6736(18)31550-2
7. Stitt AW, Curtis TM, Chen M, et al. The progress in understanding and treatment of diabetic retinopathy. *Prog Retin Eye Res*. 2016;51:156 186. https://doi.org/10.1016/j.preteyeres.2015.08.001
8. Miller JW. Developing therapies for age-related macular degeneration: the art and science of problem-solving: the 2018 Charles L. Schepens, MD, lecture. *Ophthalmol Retina*. 2019;3(10):900 909. https://doi.org/10.1016/j.oret.2019.07.015
9. Mettu PS, Allingham MJ, Cousins SW. Incomplete response to anti-VEGF therapy in neovascular AMD: exploring disease mechanisms and therapeutic opportunities. *Prog Retin Eye Res*. 2021;82:100906. https://doi.org/10.1016/j.preteyeres.2020.100906
10. Bahrami B, Hong T, Gilles MC, Chang A. Anti-VEGF therapy for diabetic eye diseases. *Asia Pac J Ophthalmol (Phila)*. 2017;6(6):535 545. https://doi.org/10.22608/apo.2017350
11. Zhang SY, Xu MJ, Wang X. Adrenomedullin 2/intermedin: a putative drug candidate for treatment of cardiometabolic diseases. *Br J Pharmacol*. 2018;175(8):1230 1240. https://doi.org/10.1111/bph.13814
12. Hong Y, Hay DL, Quirion R, Poyner DR. The pharmacology of adrenomedullin 2/intermedin. *Br J Pharmacol*. 2012;166(1):110 120. https://doi.org/10.1111/j.1476-5381.2011.01530.x
13. Wang LJ, Xiao F, Kong LM, et al. Intermedin enlarges the vascular lumen by inducing the quiescent endothelial cell proliferation. *Arterioscler Thromb Vasc Biol*. 2018;38(2):398 413. https://doi.org/10.1161/atvbaha.117.310317
14. Zhang W, Wang LJ, Xiao F, Wei Y, Ke W, Xin HB. Intermedin: a novel regulator for vascular remodeling and tumor vessel normalization by regulating vascular endothelial-cadherin and extracellular signal-regulated kinase. *Arterioscler Thromb Vasc Biol*. 2012;32(11):2721 2732. https://doi.org/10.1161/atvbaha.112.300185
15. Xiao F, Wang LJ, Zhao H, et al. Intermedin restricts vessel sprouting by inhibiting the loosening of endothelial junction. *Biochem Biophys Res Commun*. 2015;458(1):174 179. https://doi.org/10.1016/j.bbrc.2015.01.090
16. Smith LE, Wesolowski E, McLellan A, et al. Oxygen-induced retinopathy in the mouse. *Invest Ophthalmol Vis Sci*. 1994;35(1):101 111.
17. Lambert V, Lecomte J, Hansen S, et al. Laser-induced choroidal neovascularization model to study age-related macular degeneration in mice. *Nat Protoc*. 2013;8(11):2197 2211. https://doi.org/10.1038/nprot.2013.135
18. Campochiaro PA. Retinal and choroidal neovascularization. *J Cell Physiol*. 2000;184(3):301 310. https://doi.org/10.1002/1097-4652(200009)184:3<301::Aid-jcp3>3.0.Co;2-h
19. Connor KM, Krah NM, Dennison RJ, et al. Quantification of oxygen-induced retinopathy in the mouse: a model of vessel loss, vessel regrowth and pathological angiogenesis. *Nat Protoc*. 2009;4(11):1565 1573. https://doi.org/10.1038/nprot.2009.187
20. Heesterbeek TJ, Lorés-Motta L, Hoyng CB, Lechanteur YTE, den Hollander AI. Risk factors for progression of age-related macular degeneration. *Ophthalmic Physiol Opt*. 2020;40(2):140 170. https://doi.org/10.1111/opo.12675
21. Fleckenstein M, Keenan TDL, Guymer RH, et al. Age-related macular degeneration. *Nat Rev Dis Primers*. 2021;7(1):31. https://doi.org/10.1038/s41572-021-00265-2
22. Iesato Y, Toriyama Y, Sakurai T, et al. Adrenomedullin-RAMP2 system is crucially involved in retinal angiogenesis. *Am J Pathol*. 2013;182(6): 2380 2390. https://doi.org/10.1016/j.ajpath.2013.02.015
23. Valcourt U, Thuault S, Pardali K, Heldin CH, Moustakas A. Functional role of Meox2 during the epithelial cytostatic response to TGF-beta. *Mol Oncol*. 2007;1(1):55 71. https://doi.org/10.1016/j.molonc.2007.02.002
24. Cunnington RH, Northcott JM, Ghavami S, et al. The Ski-Zeb2-Meox2 pathway provides a novel mechanism for regulation of the cardiac myofibroblast phenotype. *J Cell Sci*. 2014;127(1):40 49. https://doi.org/10.1242/jcs.126722
25. Chen Y, Rabson AB, Gorski DH. MEOX2 regulates nuclear factor-kappaB activity in vascular endothelial cells through interactions with p65 and IkappaBbeta. *Cardiovasc Res*. 2010;87(4):723 731. https://doi.org/10.1093/cvr/cvq117
26. Patel S, Leal AD, Gorski DH. The homeobox gene Gax inhibits angiogenesis through inhibition of nuclear factor-kappaB-dependent endothelial cell gene expression. *Cancer Res*. 2005;65(4):1414 1424. https://doi.org/10.1158/0008-5472.Can-04-3431
27. Stahl A, Connor KM, Sapieha P, et al. The mouse retina as an angiogenesis model. *Invest Ophthalmol Vis Sci*. 2010;51(6):2813 2826. https://doi.org/10.1167/iovs.10-5176
28. Toriyama Y, Iesato Y, Imai A, et al. Pathophysiological function of endogenous calcitonin gene-related peptide in ocular vascular diseases. *Am J Pathol*. 2015;185(6):1783 1794. https://doi.org/10.1016/j.ajpath.2015.02.017
29. Zudaire E, Gambardella L, Kurcz C, Vermeren S. A computational tool for quantitative analysis of vascular networks. *PLoS One*. 2011;6(11):e27385. https://doi.org/10.1371/journal.pone.0027385
30. Izumi-Nagai K, Nagai N, Ozawa Y, et al. Interleukin-6 receptor-mediated activation of signal transducer and activator of transcription-3 (STAT3) promotes choroidal neovascularization. *Am J Pathol*. 2007;170(6):2149 2158. https://doi.org/10.2353/ajpath.2007.061018
31. Tanaka M, Kakihara S, Hirabayashi K, et al. Adrenomedullin-receptor activity-modifying protein 2 system ameliorates subretinal fibrosis by suppressing epithelial-mesenchymal transition in age-related macular degeneration. *Am J Pathol*. 2021;191(4):652 668. https://doi.org/10.1016/j.ajpath.2020.12.012
32. Imai A, Toriyama Y, Iesato Y, et al. Adrenomedullin suppresses vascular endothelial growth factor-induced vascular hyperpermeability and inflammation in retinopathy. *Am J Pathol*. 2017;187(5):999 1015. https://doi.org/10.1016/j.ajpath.2017.01.014
33. Yu HG, Liu X, Kiss S, et al. Increased choroidal neovascularization following laser induction in mice lacking lysyl oxidase-like 1. *Invest Ophthalmol Vis Sci*. 2008;49(6):2599 2605. https://doi.org/10.1167/iovs.07-1508
34. Hoerster R, Muether PS, Vierkotten S, Schroder S, Kirchhof B, Fauser S. In-vivo and ex-vivo characterization of laser-induced choroidal neovascularization variability in mice. *Graefes Arch Clin Exp Ophthalmol*. 2012;250(11): 1579 1586. https://doi.org/10.1007/s00417-012-1990-z
35. Igarashi N, Honjo M, Kaburaki T, Aihara M. Effects of ROCK inhibitors on apoptosis of corneal endothelial cells in CMV-positive Posner-Schlossman syndrome patients. *Invest Ophthalmol Vis Sci*. 2020;61(10):5. https://doi.org/10.1167/iovs.61.10.5
36. Tanaka M, Koyama T, Sakurai T, et al. The endothelial adrenomedullin-RAMP2 system regulates vascular integrity and suppresses tumour metastasis. *Cardiovasc Res*. 2016;111(4):398 409. https://doi.org/10.1093/cvr/cvw166
37. Shimekake Y, Nagata K, Ohta S, et al. Adrenomedullin stimulates two signal transduction pathways, cAMP accumulation and Ca2+ mobilization, in bovine aortic endothelial cells. *J Biol Chem*. 1995;270(9):4412 4417. https://doi.org/10.1074/jbc.270.9.4412
38. Raof NA, Rajamani D, Chu HC, et al. The effects of transfection reagent polyethyleneimine (PEI) and non-targeting control siRNAs on global gene expression in human aortic smooth muscle cells. *BMC Genomics*. 2016;17:20. https://doi.org/10.1186/s12864-015-2267-9
39. Dai K, Tanaka M, Kamiyoshi A, et al. Deficiency of the adrenomedullin-RAMP3 system suppresses metastasis through the modification of cancer-associated fibroblasts. *Oncogene*. 2020;39(9):1914 1930. https://doi.org/10.1038/s41388-019-1112-z
40. Nieto MA, Huang RY, Jackson RA, Thiery JP. EMT: 2016. *Cell*. 2016;166(1): 21 45. https://doi.org/10.1016/j.cell.2016.06.028
41. Kimura K, Orita T, Liu Y, et al. Attenuation of EMT in RPE cells and subretinal fibrosis by an RAR-γ agonist. *J Mol Med (Berl)*. 2015;93(7):749 758. https://doi.org/10.1007/s00109-015-1289-8
42. Ogoshi M, Inoue K, Takei Y. Identification of a novel adrenomedullin gene family in teleost fish. *Biochem Biophys Res Commun*. 2003;311(4):1072 1077. https://doi.org/10.1016/j.bbrc.2003.10.111
43. Takei Y, Hyodo S, Katafuchi T, Minamino N. Novel fish-derived adrenomedullin in mammals: structure and possible function. *Peptides*. 2004;25(10): 1643 1656. https://doi.org/10.1016/j.peptides.2004.06.026
44. Takei Y, Inoue K, Ogoshi M, Kawahara T, Bannai H, Miyano S. Identification of novel adrenomedullin in mammals: a potent cardiovascular and renal regulator. *FEBS Lett*. 2004;556(1-3):53 58. https://doi.org/10.1016/s0014-5793(03)01368-1
45. McLatchie LM, Fraser NJ, Main MJ, et al. RAMPs regulate the transport and ligand specificity of the calcitonin-receptor-like receptor. *Nature*. 1998;393(6683):333 339. https://doi.org/10.1038/30666
46. Lambiase A, Micera A, Sacchetti M, Cortes M, Mantelli F, Bonini S. Alterations of tear neuromediators in dry eye disease. *Arch Ophthalmol*. 2011;129(8): 981 986. https://doi.org/10.1001/archophthalmol.2011.200
47. Ito S, Fujisawa K, Sakamoto T, Ishibashi T. Elevated adrenomedullin in the vitreous of patients with diabetic retinopathy. *Ophthalmologica*. 2003;217(1): 53 57. https://doi.org/10.1159/000068244
48. Lu Y, Xu Y, Tang C. Changes in adrenomedullin in patients with proliferative diabetic retinopathy. *Curr Eye Res*. 2011;36(11):1047 1052. https://doi.org/10.3109/02713683.2011.594200
49. Udono T, Takahashi K, Takano S, Shibahara S, Tamai M. Elevated adrenomedullin in the vitreous of patients with proliferative vitreoretinopathy. *Am J Ophthalmol*. 1999;128(6):765 767. https://doi.org/10.1016/s0002-9394(99)00247-0

50. Evereklioglu C, Doganay S, Er H, Yurekli M. Aqueous humor adrenomedullin levels differ in patients with different types of glaucoma. *Jpn J Ophthalmol*. 2002;46(2):203 208. https://doi.org/10.1016/s0021-5155(01)00501-9
51. Pio R, Martinez A, Unsworth EJ, et al. Complement factor H is a serum-binding protein for adrenomedullin, and the resulting complex modulates the bioactivities of both partners. *J Biol Chem*. 2001;276(15):12292 12300. https://doi.org/10.1074/jbc.M007822200
52. Haines JL, Hauser MA, Schmidt S, et al. Complement factor H variant increases the risk of age-related macular degeneration. *Science*. 2005;308(5720): 419 421. https://doi.org/10.1126/science.1110359
53. Klein RJ, Zeiss C, Chew EY, et al. Complement factor H polymorphism in age-related macular degeneration. *Science*. 2005;308(5720):385 389. https://doi.org/10.1126/science.1109557
54. Shindo T, Kurihara Y, Nishimatsu H, et al. Vascular abnormalities and elevated blood pressure in mice lacking adrenomedullin gene. *Circulation*. 2001;104(16):1964 1971.
55. Ichikawa-Shindo Y, Sakurai T, Kamiyoshi A, et al. The GPCR modulator protein RAMP2 is essential for angiogenesis and vascular integrity. *J Clin| Invest*. 2008;118(1):29 39.
56. Guo X, Yuan J, Li M, Wang M, Lv P. Neuroprotection of intermedin against cerebral ischemia/reperfusion injury through cerebral microcirculation improvement and apoptosis inhibition. *J Mol Neurosci*. 2021;71(4):767 777. https://doi.org/10.1007/s12031-020-01697-3
57. Wang Y, Wu Z, Tian J, et al. Intermedin protects HUVECs from ischemia reperfusion injury via Wnt/β-catenin signaling pathway. *Ren Fail*. 2019;41(1): 159 166. https://doi.org/10.1080/0886022x.2019.1587468
58. Yuda K, Takahashi H, Inoue T, et al. Adrenomedullin inhibits choroidal neovascularization via CCL2 in the retinal pigment epithelium. *Am J Pathol*. 2012;181(4):1464 1472. https://doi.org/10.1016/j.ajpath.2012.06.028
59. Shu DY, Butcher E, Saint-Geniez M. EMT and EndMT: emerging roles in age-related macular degeneration. *Int J Mol Sci*. 2020;21(12):4271. https://doi.org/10.3390/ijms21124271
60. Matoba R, Morizane Y, Shiode Y, et al. Suppressive effect of AMP-activated protein kinase on the epithelial-mesenchymal transition in retinal pigment epithelial cells. *PLoS One*. 2017;12(7):e0181481. https://doi.org/10.1371/journal.pone.0181481
61. Yoshimatsu Y, Wakabayashi I, Kimuro S, et al. TNF-alpha enhances TGF-beta-induced endothelial-to-mesenchymal transition via TGF-beta signal augmentation. *Cancer Sci*. 2020;111(7):2385 2399. https://doi.org/10.1111/cas.14455
62. Luo X, Yang S, Liang J, et al. Choroidal pericytes promote subretinal fibrosis after experimental photocoagulation. *Dis Model Mech*. 2018;11(4): dmm032060. https://doi.org/10.1242/dmm.032060
63. Tenbrock L, Wolf J, Boneva S, et al. Subretinal fibrosis in neovascular age-related macular degeneration: current concepts, therapeutic avenues, and future perspectives. *Cell Tissue Res*. 2022;387(3):361 375. https://doi.org/10.1007/s00441-021-03514-8
64. Candia AF, Hu J, Crosby J, et al. Mox-1 and Mox-2 define a novel homeobox gene subfamily and are differentially expressed during early mesodermal patterning in mouse embryos. *Development*. 1992;116(4):1123 1136. https://doi.org/10.1242/dev.116.4.1123
65. Gorski DH, LePage DF, Patel CV, Copeland NG, Jenkins NA, Walsh K. Molecular cloning of a diverged homeobox gene that is rapidly down-regulated during the G0/G1 transition in vascular smooth muscle cells. *Mol Cell Biol*. 1993;13(6):3722 3733. https://doi.org/10.1128/mcb.13.6.3722-3733.1993
66. Gorski DH, Leal AJ. Inhibition of endothelial cell activation by the homeobox gene Gax. *J Surg Res*. 2003;111(1):91 99. https://doi.org/10.1016/s0022-4804(03)00042-8
67. Buchanan RA, Foley KE, Pepper KW, et al. Meox2 haploinsufficiency accelerates axonal degeneration in DBA/2J glaucoma. *Invest Ophthalmol Vis Sci*. 2019;60(10):3283 3296. https://doi.org/10.1167/iovs.18-26126
68. Liu P, Zhang C, Zhao YX, et al. Gax gene transfer inhibits vascular remodeling induced by adventitial inflammation in rabbits. *Atherosclerosis*. 2010;212(2): 398 405. https://doi.org/10.1016/j.atherosclerosis.2010.06.001
69. Ricci F, Bandello F, Navarra P, Staurenghi G, Stumpp M, Zarbin M. Neovascular age-related macular degeneration: therapeutic management and new-upcoming approaches. *Int J Mol Sci*. 2020;21(21):8242. https://doi.org/10.3390/ijms21218242